AD-A013 779

STUDY, DESIGN AND FABRICATE A COLD CRUCIBLE SYSTEM

Joseph F. Wenckus, et al

Arthur D. Little, Incorporated

Prepared for:

Air Force Cambridge Research Laboratories

31 March 1975

Best Available Copy

240120

AFCRL-TR-75-0213

AD A013779

STUDY, DESIGN AND FABRICATE A COLD CRUCIBLE SYSTEM

Joseph F. Wenckus
Martin L. Cohen
Alfred G. Emslie
Wilson P. Menashi
Peter F. Strong

Arthur D. Little, Inc.
15 Acorn Park
Cambridge, Massachusetts 02140

31 March 1975

Final Report for Period

1 November 1973 - 28 February 1975

Approved for public release; distribution unlimited.

AIR FORCE CAMBRIDGE RESEARCH LABORATORIES
AIR FORCE SYSTEMS COMMAND
UNITED STATES AIR FORCE
HANSCOM AFB, MASSACHUSETTS 01731

SECURITY CLASSIFICATION OF THIS PAGE (When Data Entered)

REPORT DOCUMENTATION PAGE		READ INSTRUCTIONS BEFORE COMPLETING FORM
1. REPORT NUMBER AFCRL-TR-75-0213	2. GOVT ACCESSION NO.	3. RECIPIENT'S CATALOG NUMBER
4. TITLE (and Subtitle) STUDY, DESIGN AND FABRICATE A COLD CRUCIBLE SYSTEM		5. TYPE OF REPORT & PERIOD COVERED Final Report for period 1 Nov. 73 - 28 Feb. 75
		6. PERFORMING ORG. REPORT NUMBER
7. AUTHOR(s) Joseph F. Wenckus, Martin L. Cohen, Alfred G. Emslie, Wilson P. Menashi, Peter F. Strong		8. CONTRACT OR GRANT NUMBER(s) F19628-74-C-0097
9. PERFORMING ORGANIZATION NAME AND ADDRESS Arthur D. Little, Inc. 15 Acorn Park, Cambridge, MA 02140		10. PROGRAM ELEMENT, PROJECT, TASK AREA & WORK UNIT NUMBERS 5620-09-06 61102F
11. CONTROLLING OFFICE NAME AND ADDRESS Air Force Cambridge Research Laboratories Hanscom AFB, MA 01731 Contract Monitor: Dr. Joseph J. Hutta/LQP		12. REPORT DATE 31 March 1975
		13. NUMBER OF PAGES 73
14. MONITORING AGENCY NAME & ADDRESS(if different from Controlling Office)		15. SECURITY CLASS. (of this report) Unclassified
		15a. DECLASSIFICATION/DOWNGRADING SCHEDULE
16. DISTRIBUTION STATEMENT (of this Report)		
17. DISTRIBUTION STATEMENT (of the abstract entered in Block 20, if different from Report)		
18. SUPPLEMENTARY NOTES Tech., Other		
19. KEY WORDS (Continue on reverse side if necessary and identify by block number) Cold Crucible System, Semiconductors, Oxides		

20. ABSTRACT (Continue on reverse side if necessary and identify by block number)

The objective of this program was to conduct a study, design and fabricate a cold crucible system for the synthesis and crystal growth of refractory semiconductors and oxides. A theoretical analysis of the cold crucible relating the properties of the material to the electrical characteristics of the cold crucible was completed. The thermal analysis, which includes thermal modeling by means of a computer technique, was also completed. A detailed analysis of the RF power control system necessary to provide the

DD FORM 1 JAN 73 1473 EDITION OF 1 NOV 65 IS OBSOLETE

Unclassified

SECURITY CLASSIFICATION OF THIS PAGE (When Data Entered) desired stability for crystal growth was also carried out.

A cold crucible assembly suitable for the growth of refractory oxide crystal has been designed and constructed. It is a simple, rugged modular assembly which will be readily adapted in the future to a [illegible] atmosphere furnace system.

Using a 50 Kw (4-7 megahertz) RF power supply manufactured by Fritz Huettinger Elektronik GmbH, Freiburg, Germany, the cold crucible assembly was tested and kilogram melts of zirconia (melting point 2690°C) were successfully contained.

The cold crucible assembly developed during the course of this program was delivered to Air Force Cambridge Research Laboratories (LQP).

TECHNICAL SUMMARY

The objectives of this program were the study, design and fabrication of a cold crucible system for the synthesis and crystal growth of refractory semiconductors and oxides. The work performed during the course of this program and the results achieved may be summarized briefly as follows:

- Theoretical analysis of the electrical characteristics of the cold crucible system.

  It was found that a properly designed skull melting assembly has no effect on the field applied to the charge. The skull merely lowers the inductance of the RF coil slightly by excluding the field from the volume occupied by the tube structure and adds a small resistive loading to the coil.

  The power delivered to the molten charge by a given RF field was calculated for disc-shaped charges approximated by an ellipsoid of revolution. These calculations were carried out for both large and small field penetration skin depths and, for an ellipsoid of dimensions 8cm x 8cm x 2cm in a field of 1000 A/m, the maximum power required is several kilowatts.

  In considering skull melting assemblies of varying sizes, our analysis shows that, for skin depths which are small compared to the radius of the skull, the power required is generally proportional to the square of the radius. However, in the case where skin depth is large compared to the skull radius, the RF power must be transferred at a high field and therefore lower overall efficiency. In general, large cold crucible assemblies appear to be more efficient than small systems.

° Theoretical analysis of the thermal characteristics of the cold crucible system.

Using computer techniques for thermal modeling of various skull melting configurations, we found that the molten region tends to take the shape of a flattened body of revolution. With the source of heat near the equatorial plane near the surface of the body, heat travels inwards and is lost by radiation and conduction along the way.

If a substantial heat loss from the melt surface occurs, the shape of the melt is very sensitive to the amount thus lost. Therefore, upper radiation shielding is vital to the stability of melt temperature.

° A detailed analysis of the RF power control system necessary to provide the desired stability of operation.

A closed loop control system was used to maintain constant power input to the melt. Initially, RF current feedback control was explored but improved control of RF power was achieved by using the oscillator plate current as the feedback signal.

The response time of the control system was approximately 2 seconds; however, the thermal time constant of the molten charge was much longer than this with the result that melt temperature fluctuations due to external disturbances were relatively small.

° Design and construction of a cold crucible assembly suitable for the growth of refractory oxides.

The resultant design was based upon the guidelines established by the theoretical analysis as well as first-hand knowledge of the cold crucible configurations which are currently operating with considerable success in the U.S.S.R. The cold crucible system developed is a rugged, completely metallic, modular assembly which will be readily adaptable in the future to a controlled atmosphere furnace system; indeed, the structure has been designed to withstand external operating pressures up to 100 atmospheres.

°Testing and evaluation of the cold crucible assembly using stabilized zirconia (melting point 2690°C).

Over thirty (30) melting experiments were carried out in the cold crucible assembly. The power supply used was a 50 kilowatt high frequency RF generator (manufactured by Fritz Huettinger Elektronik GmbH, Freiburg, Germany) tuned to operate at approximately 4 megahertz.

Using kilogram charges of zirconia powder, densification and melting could be achieved with applied RF power levels as low as 6 kilowatts. At 15 kilowatts of applied power, it was possible to obtain complete, stable melting of the zirconia charge.

Large, semitransparent columnar grain single crystals of stabilized zirconia (typically 3-4mm on edge by 5-7mm in length) were obtained by slow cooling of melts contained in the cold crucible assembly.

°Development of the criteria for integration of the cold crucible assembly within a controlled atmosphere, high pressure furnace chamber.

One major concern was the effect of electrical grounding on the performance of the cold crucible. It was found that stable melts could be achieved and maintained quite readily whether the cold crucible was grounded or not to the RF power supply.

As noted above, the cold crucible assembly has been designed for operation at external pressures up to 100 atmospheres.

The major problem, as yet unresolved, involves the development of a low-loss coaxial RF feedthrough designed not only to provide maximum RF transmission at megahertz-frequencies but which meets the requirements for safe operation at high pressures (approximately 100 atmospheres).

°Upon completion of the program, the prototype of the cold crucible assembly was delivered to the Air Force Cambridge Research Laboratories (LQP).

PREFACE

Major advances in the development of cold crucibles, i.e. water cooled metal crucibles for use with RF induction heating, used for "skull melting", have taken place in the past two years with significant impact on refractory materials technology. For the first time, it is possible to contain stable, uncontaminated melts of even the most refractory materials for which no crucible exists.

Russian scientists at the Lebedev Physical Institute in Moscow have developed skull melting to a point where is has become a reproducible production operation. Oxide melts at temperatures up to 3000°C with weights up to 25 kilograms are being used in the production of a wide variety of strategic materials including unique laser crystals, refractory optical elements and melt-cast ceramics.

The new process involves direct high frequency induction heating of the material contained in a water cooled, crucible-like structure. The melt formed is contained by a sintered shell or "skull" of identical composition so that the problems of reaction and contamination, traditionally the most severe problem faced in the containment of refractory melts, have been virtually eliminated. The melt can then be cast or recrystallized using standard methods of crystal growth.

TABLE OF CONTENTS

LIST OF ILLUSTRATIONS

LIST OF TABLES

1.0 INTRODUCTION

The principal objective of the program was the design and development of of a skull melting system which can be used for the production of high purity oxide single crystals. Typically, most of the cold crucibles in operation today have evolved by empirical trial and error procedures. A theoretical analysis of the cold crucible has been carried out to relate the properties of the material(s) to be melted to the electrical and thermal characteristics of the cold crucible. Based upon this analysis we have established basic guidelines for the design and construction of cold crucible assemblies.

One of the major problems as yet unresolved in the use of the cold crucible for the growth of single crystals is related to the stabilization and precise control of melt temperature. We have analyzed the critical control parameters of the cold crucible and, based upon the unique RF power control techniques which have been developed in the United States, have defined a control system to provide the high degree of stability necessary for crystal growing applications.

A cold crucible assembly complete with control system suitable for oxide crystal growing operation has been designed and constructed. Testing and evaluation of the cold crucible assembly and control system have been carried out to explore the operating techniques suitable for crystal growing applications. Stabilized zirconia (melting point 2690°C) has been used to demonstrate the very high temperature operation of the cold crucible under oxidizing conditions. Large columnar crystal grains of partially stabilized zirconia have been recrystallized from stable melts contained in the cold crucible.

The ultimate goal of this work is the integration of the cold crucible system into a crystal growing furnace chamber capable of operation under controled atmospheres at pressures up to 100 atmospheres.

It appears that no difficulties will be encountered with the integration of the cold crucible inside the high pressure furnace chamber. However, it will be necessary to develop a suitable coaxial high frequency RF transmission line for the furnace which will satisfy the requirements of the ASME Pressure Vessel Codes as well as the requirements for low loss RF power transmission.

2.0 TECHNICAL DISCUSSION

2.1 INTRODUCTION

During the course of this program we have:

1. Theoretically analyzed the electrical characteristics of the cold crucible system. The problems involved and the conclusions derived are presented in Section 2.2 while the derivation is discussed in Appendix A.

2. Theoretically analyzed the thermal characteristics of the cold crucible. The conclusions are presented in Section 2.3 and the derivation shown in Appendix B.

3. Theoretically analyzed the control of the RF power. This is discussed in Section 2.4 and the derivation is presented in Appendix C.

4. Designed and constructed the cold crucible assembly. Refer to Section 2.5 for review of the design criteria.

5. Tested the cold crucible assembly with stabilized zirconia (melting point 2690°C) for demonstration purposes. Operating procedures and results are reviewed in Section 2.6.

6. Investigated the criteria for integration of the cold crucible assembly in a high pressure furnace chamber. Section 2.7 reviews the problems involved.

7. Delivered a cold crucible assembly to the Air Force Cambridge Research Laboratories (LQP).

2.2 THEORETICAL ANALYSIS OF THE ELECTRICAL CHARACTERISTICS OF THE COLD CRUCIBLE

The following problems involved in skull melting of refractory materials have been theoretically analyzed:

°The effect of the copper cage on the magnetic field applied to the refractory charge.

°The resistive and inductive effects of the cage on the radio frequency coil.

°The effect of the skin depth of field penetration on the total power input to the charge.

°The spatial distribution of the power input.

°The resistive loading of the RF coil due to power absorbed by the charge.

°The RF magnetic field required to melt metal particles in the charge to achieve startup.

°The effects of scaling the size of the cold crucible assembly on the applied magnetic field as related to skin depth.

It is found that a properly designed cage has no effect on the field applied to the charge. The cage merely lowers the inductance of the RF coil slightly by excluding the field from the volume occupied by the cage tubing and adds a small resistive loading to the coil.

The power delivered to the molten charge by a given applied RF field is calculated for a disc-shaped charge approximated by an ellipsoid of revolution. This is done for the field penetration skin depth both large and small compared with the smallest semi-axis of the ellipsoid. These two limiting cases converge twoard a common maximum value of the power when the skin depth in each case approaches the size of the semi-axis. For an ellipsoid of dimensions 8cm x 8cm x 2cm in a field of 1000 A/m, this maximum power is several kilowatts.

The calculations show that the heating power is strongly concentrated around the equator of the ellipsoid, especially when the skin depth is small compared with the thickness of the ellipsoid. An expression is derived for the resistive loading of the RF coil by the induced currents in the molten charge.

Startup by means of 2mm diameter metal spheres embedded in the powdered charge is found to be theoretically feasible but requires a starting field perhaps 10 times larger than that needed to maintain the melt.

Our analysis shows that for skin depths which are small compared to the radius of the skull, the power required is generally proportional to the square of the radius. However, in the case where the skin depth is large compared to the radius, then the power must be transferred at a higher field and therefore reduced overall efficiency. The conductivity of ZrO_2 (1,2) is approximately 10 Mho/cm at its melting point and approximately .35 Mho/cm at about 1300°C with a reasonably linear relationship. At a frequency of 3.5 megacycles the skin depth is 0.85cm at its melting point and 5cm at 1300°C. Therefore the skull constructed with a diameter of approximately 7cm will couple very easily at the melting point but will exhibit reduced coupling efficiency at 1300°C. If the material to be melted has a conductivity vs. temperature profile as shown in Figure 1 for Al_2O_3 (3), the dramatic change in conductivity (over 2 orders of magnitude) shows that control of this material at or near the melting point is quite critical. Once the alumina has solidified, the coupling efficiency will be so poor that it cannot be remelted.

2.3 THERMAL ANALYSIS OF THE COLD CRUCIBLE

The thermal analysis of the feed powder and the melt when heated by the induced RF currents and cooled by the walls of the container was completed. We find that:

°The molten region tends to take the shape of a flattened body of revolution; it acts as a fin, with the source of heat in a ring near the equatorial plane near the surface of the body. Heat travels inwards and is lost by radiation and conduction along the way.

°If a substantial heat loss from the top surface of the melt occurs, the shape of the melt is very sensitive to the amount thus lost.

°There should be a large amount of powder to insulate the melt on its underside, although the exact amount is not critical. This means that the molten zone should be confined to the upper portion of the cooled container.

Thermal models have been developed for typical skull melting systems and the effects of heat sources and sinks upon melt shape have been profiled by computer techniques and are discussed in Appendix B.

2.4 CONTROL OF RF POWER

Stable control of the RF power is required for successful crystal growth. There is a basic tendency toward instability when induction heating is used directly to melt semiconductors and refractory oxides. Therefore a closed loop control system was used to maintain a constant power input to the melt. Initially RF current feedback control was explored but improved control of RF power into the contained melt was achieved by the use of the oscillator plate current as the feedback signal.

After melting, the balance between heat generation and heat loss processes results in a stable system. The response time of the control system was about 2 seconds. The thermal time constant of the charge was much longer than this, with the result that temperature fluctuations due to external disturbances were relatively small.

Using a 50 kilowatt output high frequency RF power supply, we would obtain fields stronger than 10^4 amperes per meter, which were sufficient to melt kilogram charges of stabilized zirconia and maintain them in the fully molten state.

2.5 DESIGN AND CONSTRUCTION OF THE COLD CRUCIBLE ASSEMBLY

Based upon the electrical and thermal analyses which have been carried out, we completed the design of a cold crucible assembly which is shown in Figure 2. The copper structure has been designed for high pressure operation and integration with the ADL crystal growing furnaces presently in use at the Air Force Cambridge Research Laboratories. The cold crucible assembly is shown in Figures 3 and 4.

2.6 TESTING OF THE COLD CRUCIBLE ASSEMBLY

During the course of the testing and evaluation phase of the program, over thirty (30) melting experiments were carried out in the cold crucible assembly. The power supply used was a 50 kilowatt high frequency RF power supply manufactured by Fritz Huettinger Elektronik GmbH, Freiburg, Germany, tuned to operate at approximately 4 megahertz. The cold crucible in operation with a 1 kilogram charge of stabilized zirconia is shown in Figure 5.

To set up the cold crucible for operation, the assembly is first wrapped in Fiberfrax on the outside (to prevent loss of feed powder from between the tubes). The Fiberfrax is held in place by a quartz or pyrex tube. Cooling water is supplied to the skull at the rate of 3 gallons per minute.

The skull was filled with stabilized zirconia powder and approximately 10 grams of zirconium metal chips (1/8" diameter) were buried in the center of the powder. The RF power (approximately 4 megahertz) was then turned on and increased to an indicated plate voltage of approximately 4-5 kilovolts. Within 10 minutes the zirconium chips would become incandescent and heat the surrounding powder charge. As the zirconia charge heated, the plate voltage dropped and the current increased, indicating more efficient coupling due to the increase in electrical conductivity of the heated zirconia. As the RF coupling increased, the powder would densify and melt and it was necessary to add more powder to the molten charge.

While densification and melting could be initiated with RF power levels as low as 6 kilowatts, applied RF power in excess of 15 kilowatts produced better results.

Figure 6 shows a fused stabilized zirconia (Zircoa Corporation) charge as removed from the cold crucible assembly. Note that the outer sintered shell of the charge (approximately 1mm thick) has retained the shape of the multi-tube structure of the cold crucible. The top of the molten charge shows the effects of continuous out-gassing during the course of the fusion operation. No external radiation shield was used to reduce the severe radiation losses from the upper surface of the molten charge, and a solid, translucent crust formed above the melt which had to be repeatedly punctured to permit the addition of feed powder.

Figure 7 shows the initiation of melting using approximately 6 kilowatts of applied RF power to the charge. Note the sintered dark mass near the bottom where the zirconium charges were placed. It is also evident that once heating starts, the last place to heat is the center region. Figure 8 shows Sample 3 with an input power of 7 kilowatts; clearly more sintering and melting is evident. Figure 9 shows Sample 7 with an input of 9 kilowatts power. First evidence of melting is now obviously visible near the top of the charge.

It was evident that some form of radiation shielding was required to reduce thermal losses from the incandescent melt and to minimize the hard crust formation above the melt surface. A zirconia ceramic radiation shield was positioned on top of the cold crucible structure. However, it was noted that, with the RF load coil positioned close to the top of the cold crucible, the hot ceramic radiation shield was heated inductively, thus reducing the total power available to fuse the charge and destroying the radiation shield.

Figure 10 is an example of fusion (charge M-2) with the coil near the top of the cold crucible. Note that while better melting was observed, crust formation was still appreciable. In this run the radiation shield was destroyed. In Figure 11 (Sample M-3), the coil was substantially lowered, showing significantly less crust formation; the shield remained intact

The decision was made to reduce the size of the charge to approximately 700 grams (thus lowering the melt level) and to lower the RF coil so that the lowest turn was positioned at the bottom of the cold crucible. Subsequent experiments using ceramic radiation shielding (Norton sintered zirconia bubble plate) proved to be quite satisfactory and melts could be readily maintained with significantly reduced crust formation.

Figure 12 (Sample M-9) was run using Y_2O_3 stabilized zirconia and cooled to room temperature over 1 hour. The sample had a distinct yellow color, but large columnar transparent grains were evident.

Figures 13 and 14 show the results of Run M-10. A 700 gram zirconia powder charge (Johnson Matthey Chemicals, Ltd., 99.99% purity) was used with 10 wt % yttria (Rare Earth Products, Ltd., 99.99% purity) added to prevent the destructive phase change (cubic to tetragonal to monoclinic) which occurs during the high temperature recrystallization of zirconia.

The charge was melted with 15 kilowatts of applied RF power (estimated loss via radiation is less than 2 kilowatts). The melt was cooled slowly over a period of 1 hour and, upon removing the recrystallized charge from the cold crucible, large, semitransparent columnar crystals of zirconia were revealed. Upon visual examination of the columnar crystals (typically 2-3mm on edge and 5-6mm in length) translucent regions were dispersed throughout the transparent grains indicating that the high temperature cubic-phase was not fully stabilized; it appears that more than 10 wt % yttria should be added to the zirconia charge to fully stabilize the cubic form.

With regard to the use of automatic RF power control, it was found that the automatic control system could not be utilized effectively during the heating or cooling phases of the melting operation. At the critical temperature where the skin depth of the charge was approximately that of the cold crucible, the RF coupling efficiency would change drastically, thus causing the control circuit to overdrive the RF generator. Once the stable melt had been achieved (using manual control methods) the RF power control system proved to be very effective in maintaining a stable power input to the fused mass. At the termination of the experiment, the cooling operation was carried out by manually reducing the input power.

2.7 INTEGRATION OF THE COLD CRUCIBLE ASSEMBLY WITH A HIGH PRESSURE FURNACE

To date, all of the melting experiments with the cold crucible assembly have been carried out in air (as shown in Figure 5) and there are obvious advantages to using this assembly within a controlled atmosphere, high pressure furnace chamber.

One major concern was the effect of electrical grounding on the performance of the cold crucible. The cold crucible has been operated both with and without grounding to the RF power supply and stable melts could be achieved quite readily in either case.

The cold crucible assembly was designed initially so that the support stem could be sealed into the base port of the standard ADL Model MP, HP or HPCZ Furnaces. An O-ring sealed support structure (to adapt the cold crucible to these furnaces) has been designed to permit operation at pressures ranging from 10^{-5} torr to 100 atmospheres. The cold crucible assembly could easily be mounted in a fixed position at the base of the furnace to facilitate Czochralski crystal growing experiments. Alternatively, the stem of the cold crucible assembly could be attached to a lower drive mechanism, thus permitting vertical movement of the assembly for Bridgman-type crystal growing operations.

In order to fuse large melts (of the order of 1 kilogram), it will be necessary to add feed powder to the cold crucible assembly during the course of the melt-down operation. A suitable powder storage vessel and feed mechanism, capable of operating at gas pressures up to 100 atmospheres, have been designed for glass-melting applications prior to the initiation of this program and should prove to be useful in resolving this operating problem.

The major difficulty we can foresee in integrating the cold crucible assembly within a controlled atmosphere furnace chamber involves the low-loss transmission of high frequency (megahertz range) RF power into the sealed metal chamber. It will be necessary to design a suitable coaxial RF feedthrough which will not only provide maximum RF transmission efficiency but meet the requirements for safe operation at high pressures (approximately 100 atmospheres).

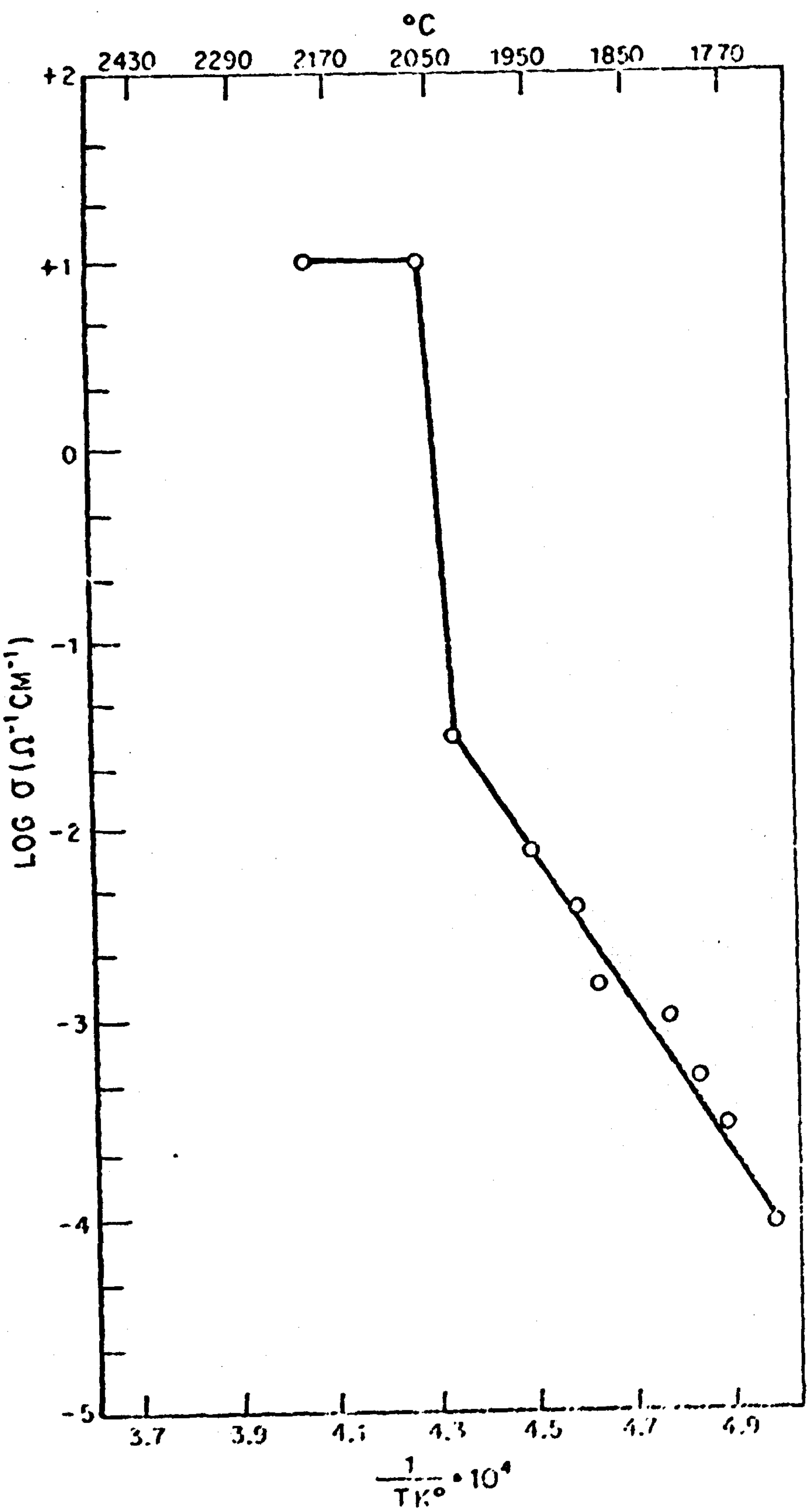

FIGURE 1. TEMPERATURE DEPENDENCE OF ELECTRICAL CONDUCTIVITY OF Al_2O_3.

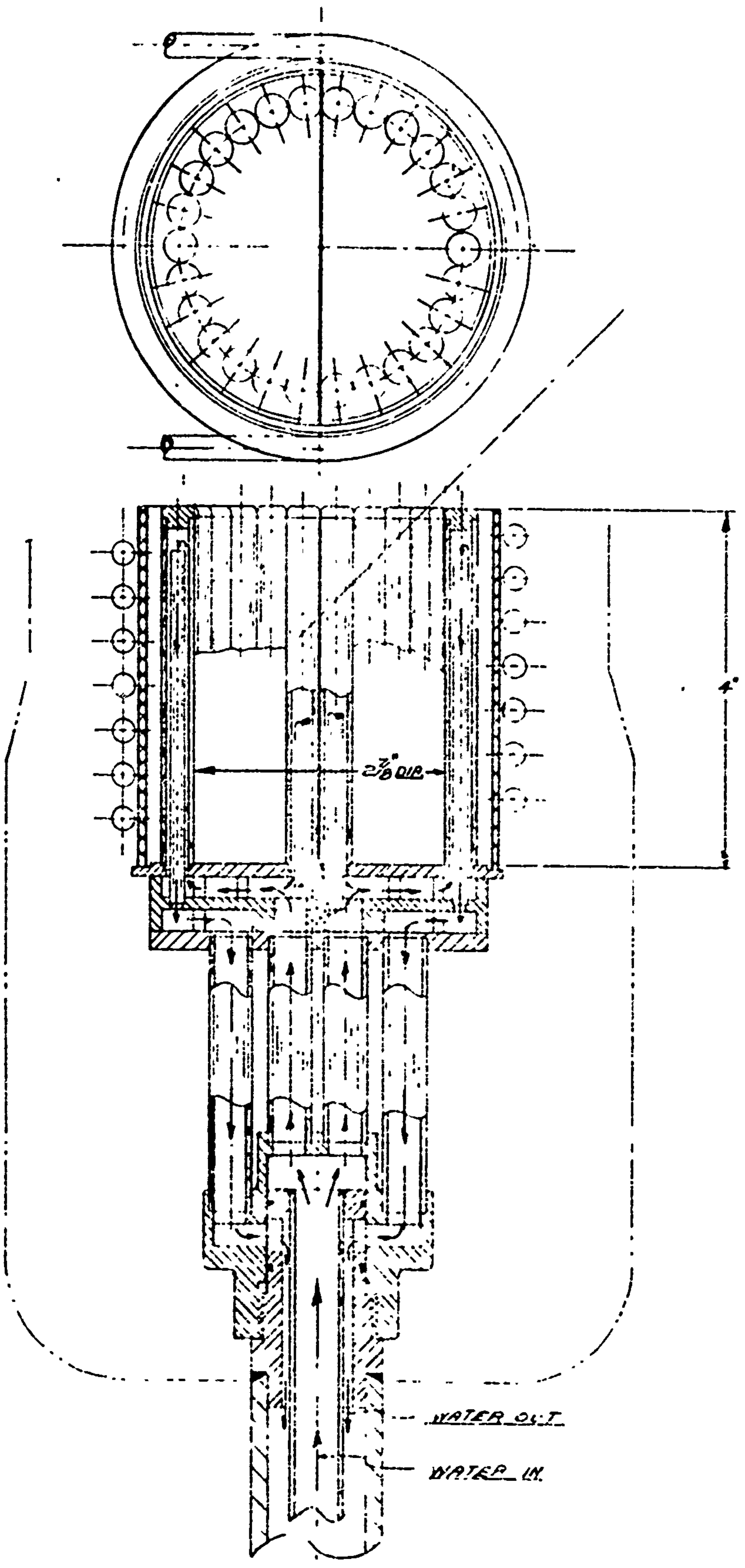

FIGURE 2 SCHEMATIC DRAWING OF THE ADL COLD CRUCIBLE ASSEMBLY

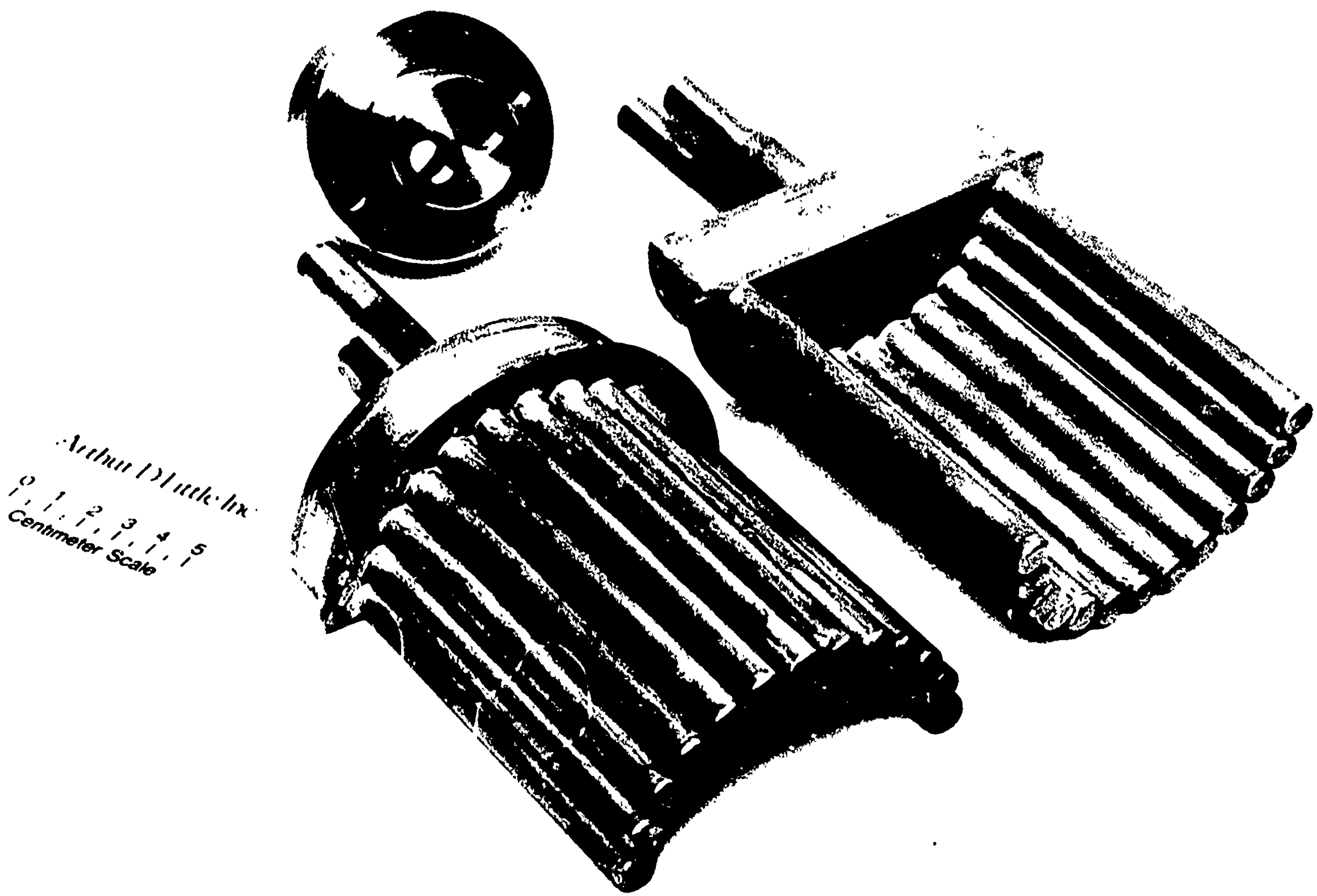

FIGURE 3 ADL COLD CRUCIBLE ASSEMBLY - SECTIONED

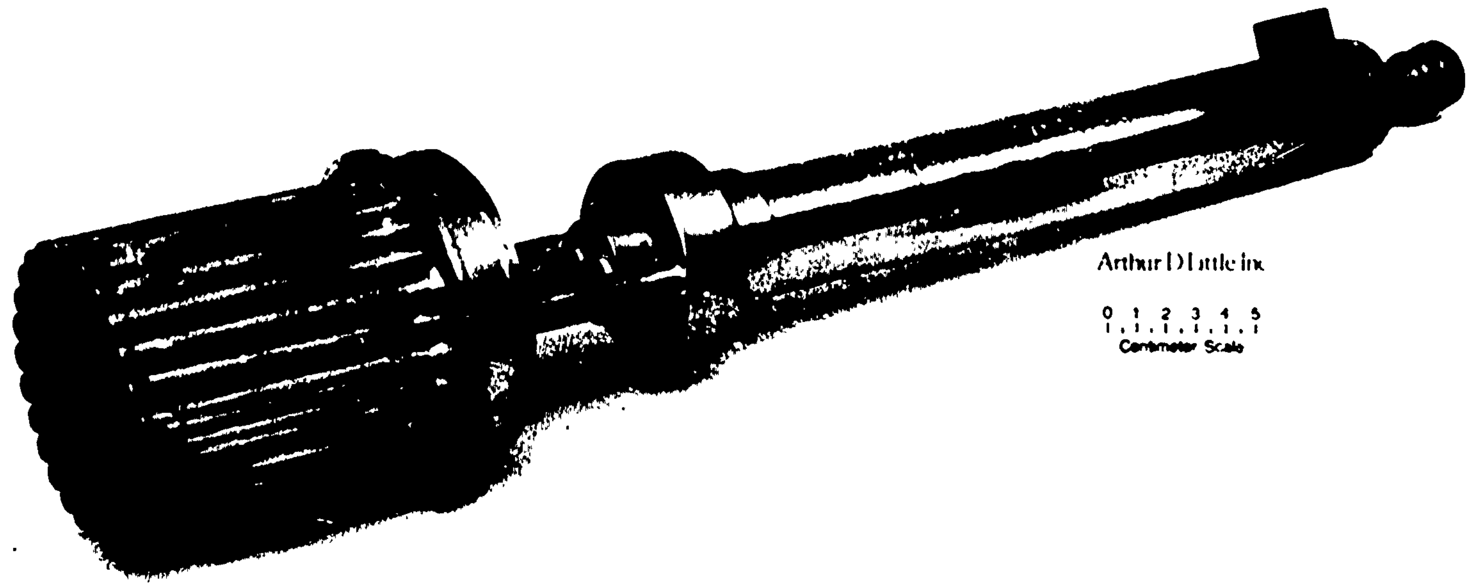

FIGURE 4 ADL COLD CRUCIBLE ASSEMBLY

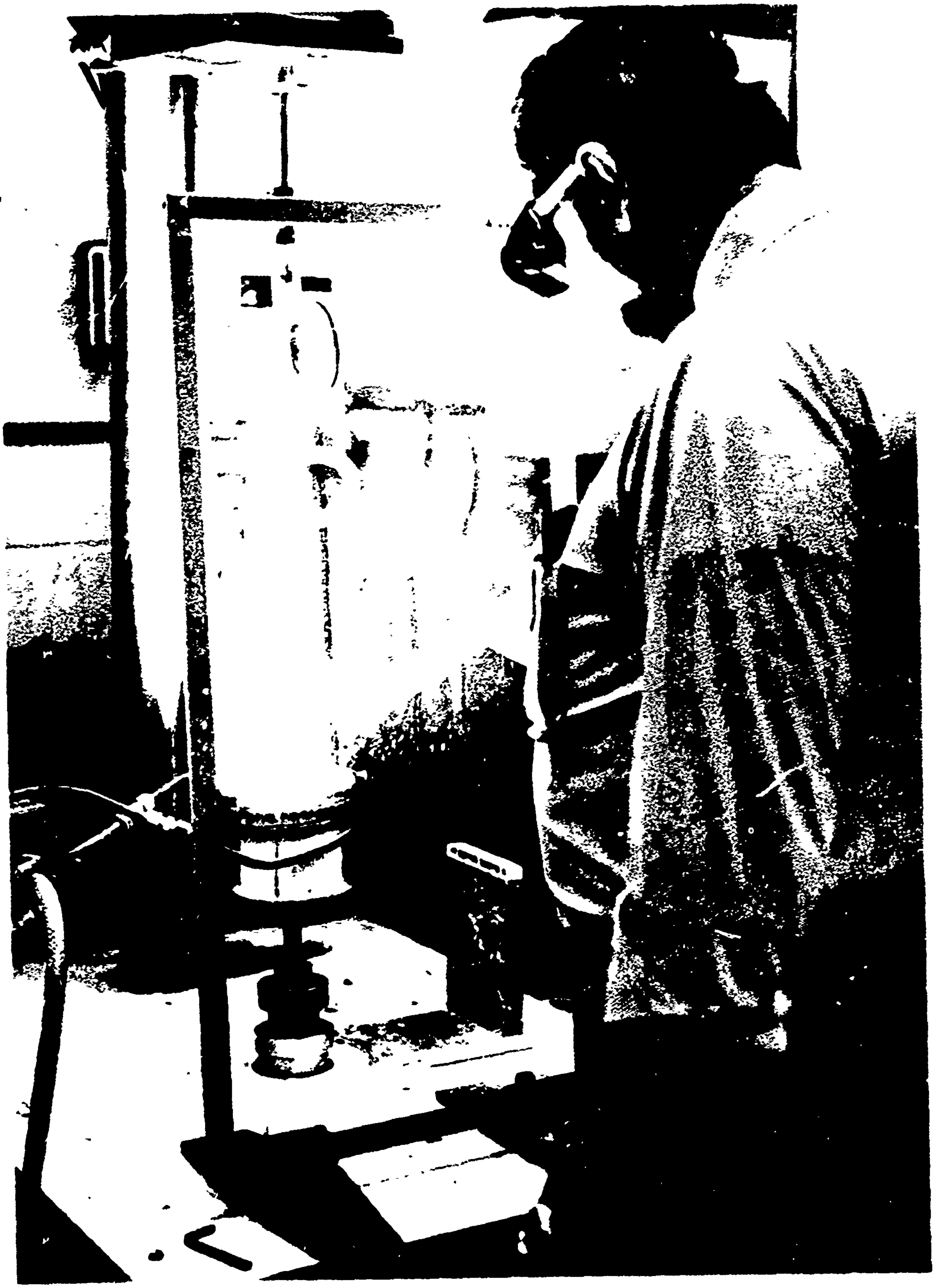

FIGURE 5 ADL COLD CRUCIBLE ASSEMBLY IN OPERATION

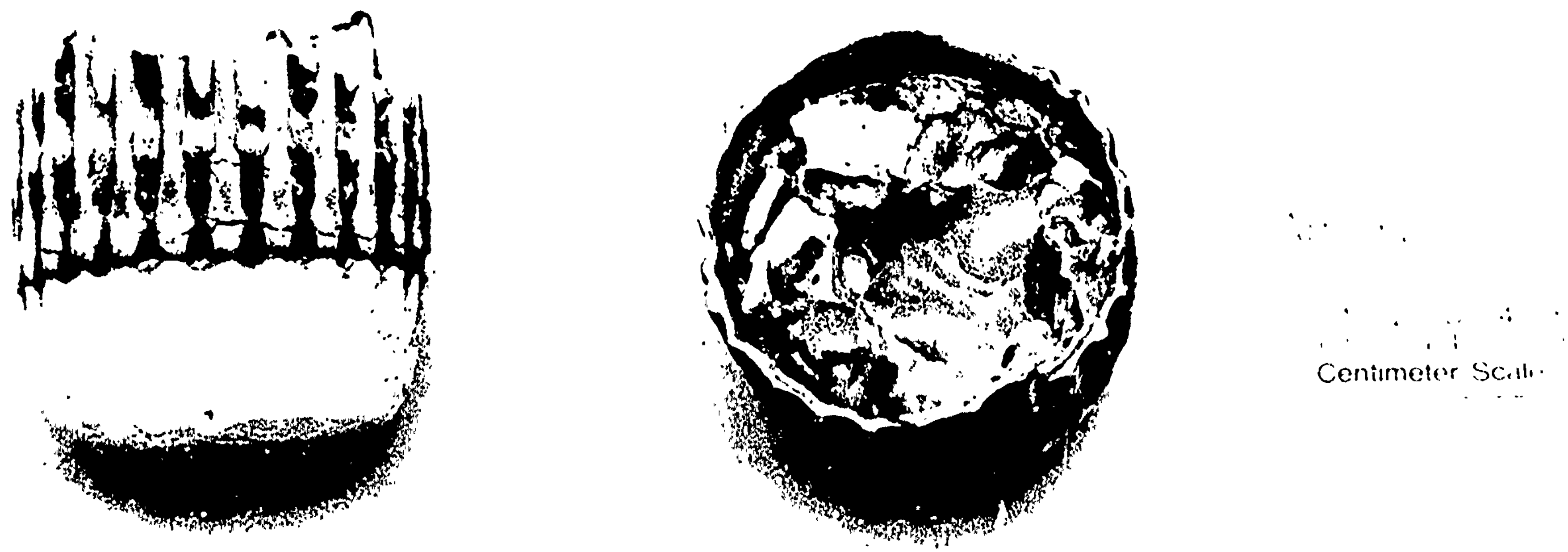

FIGURE 6 FUSED ZIRCONIA CHARGE REMOVED FROM ADL COLD CRUCIBLE ASSEMBLY SHOWING THE MULTI-TUBE STRUCTURE

FIGURE 7 FUSED ZIRCONIA CHARGE SHOWING FIRST INDICATIONS OF MELTING

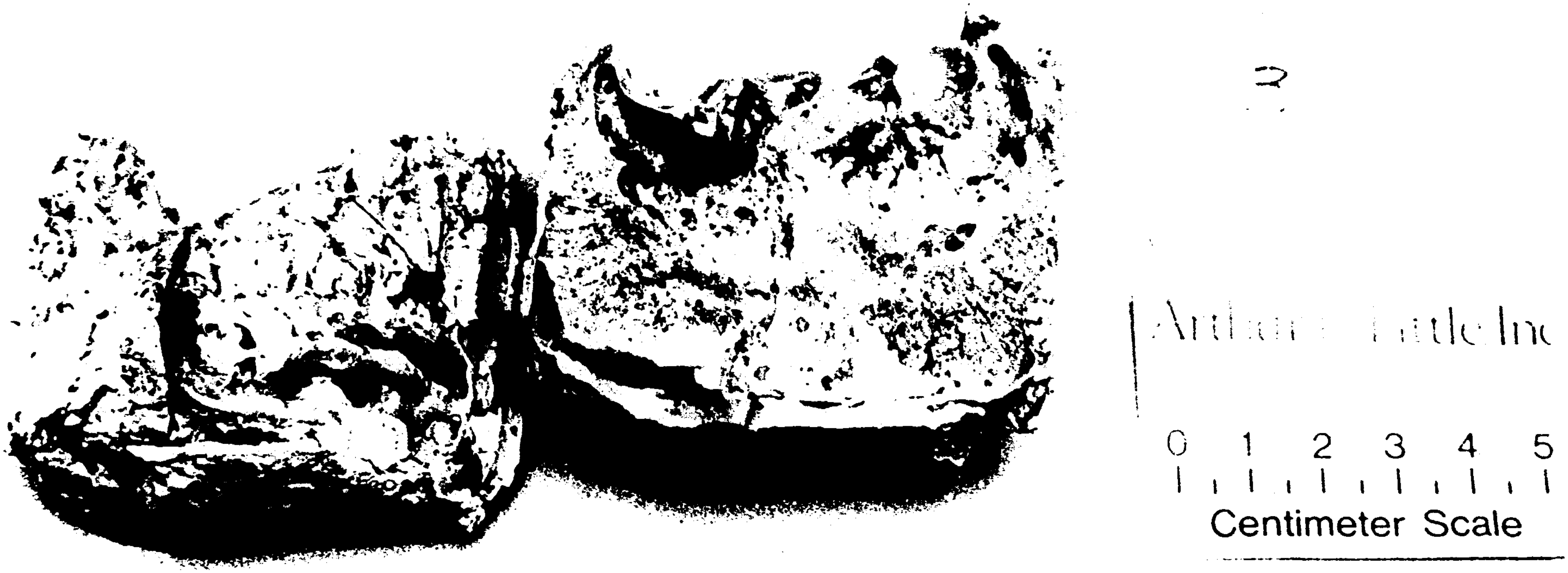

FIGURE 8 ZIRCONIA CHARGE FUSED WITH APPROXIMATELY 7 KW RF POWER

FIGURE 9 ZIRCONIA CHARGE FUSED WITH APPROXIMATELY 9 KW RF POWER

FIGURE 10 ZIRCONIA CHARGE FUSED WITH APPROXIMATELY 11 KW RF POWER (RF COIL POSITIONED NEAR THE TOP OF THE CHARGE)

FIGURE 11 ZIRCONIA CHARGE FUSED WITH APPROXIMATELY 11 KW RF POWER (RF COIL NEAR THE BOTTOM OF THE COLD CRUCIBLE)

FIGURE 12 ZIRCONIA CHARGE FUSED WITH APPROXIMATELY 15 KW RF POWER

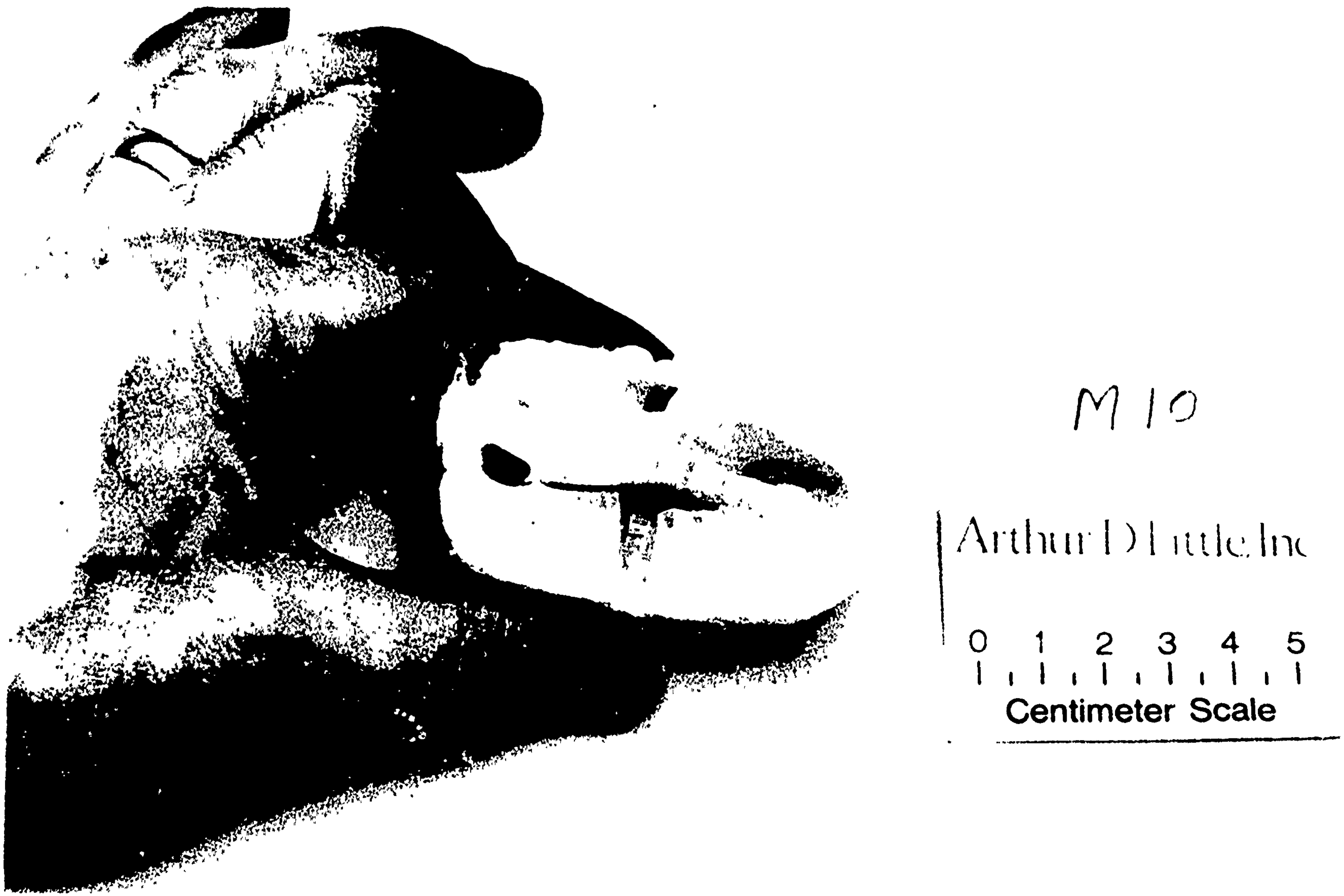

FIGURE 13 ZIRCONIA CHARGE (99.99% PURITY) FUSED AT APPROXIMATELY 15 KW RF POWER

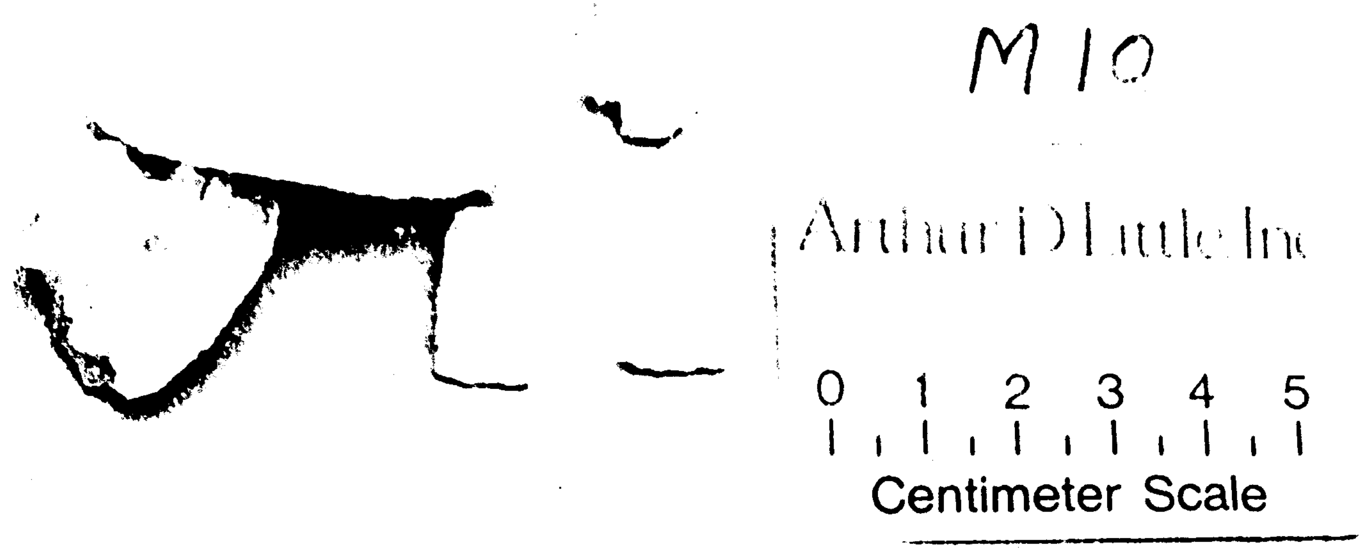

FIGURE 14 COLUMNAR GRAINS OF ZIRCONIA OBTAINED ON SLOW COOLING

5.0 CONCLUSIONS

°A simple, rugged cold crucible assembly has been developed which can be used to contain stable kilogram size, refractory oxide melts at temperatures up to 3000°C in air.

°Theoretical analyses of the thermal and electrical characteristics of cold crucible operation have been carried out and verified experimentally. Based upon these analyses we have established the basic guidelines for the design and construction of cold crucible assemblies.

°The critical control parameters of the cold crucible have been developed and we have defined an RF power control system necessary to provide the high degree of stability for crystal growing operations.

°The cold crucible assembly has been designed and constructed to withstand external pressures up to 100 atmospheres and we have established the criteria for integration of the cold crucible assembly within a high pressure furnace chamber.

4.0 RECOMMENDATIONS

Theoretical analysis of cold crucible melting and processing indicates that minimal problems will be encountered in developing large-scale cold crucible systems. There is already dramatic evidence of the potential industrial applications of this new technology; Russian workers[3] have successfully contained refractory oxide melts weighing up to 25 kilograms and molten glass charges up to 250 kilograms in weight are now being processed in France.[6]

To date most cold crucible operations are carried out in air. Under controlled atmosphere conditions, this new process may well be the answer to the time honored problems of working with ultra-refractory materials such as ferrites, semiconductors, chalcogenide-glasses, metal alloys and cermets whose melts are sensitive to ambient atmosphere composition or pressure.

It appears that few difficulties will be encountered with the integration of the cold crucible system inside . high pressure furnace chamber. However, it will be necessary to develop a suitable coaxial high frequency RF transmission line for the furnace which will satisfy the stringent requirements of high pressure operation and minimal RF power loss.

APPENDIX A

THEORETICAL ANALYSIS OF THE ELECTRICAL CHARACTERISTICS OF SKULL MELTING

A.1 EFFECT OF THE CAGE

We assume that the cage consists of vertical copper tubes parallel to the axis of the coil as shown in cross section in Figure A.1. The effect of the bottom of the cage is small and will be neglected here.

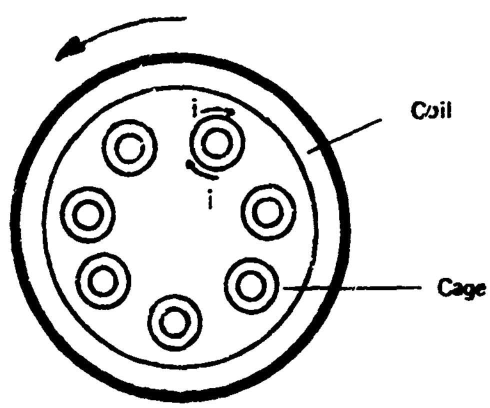

CROSS SECTION OF SKULL MELTING CAGE

FIGURE A.1

If the coil has n turns and a length ℓ and carries an alternating current, I, the rms current per unit length is

$$i = \frac{nI}{\ell} \text{ (A/m)} \quad (1)$$

and the axial magnetic field is

$$H_o = \frac{nI}{\ell} \text{ (A/m)} \quad (2)$$

At frequencies in the range 1-10 megahertz, the skin depth of penetration of the field into the copper tubes of the cage is only about 2×10^{-5} m. The copper therefore essentially excludes the field and acts like an almost perfect diamagnetic material. Under these conditions each tube has a circulating current per unit length equal to -i (A/m).

The energy stored in the field is

$$E = \frac{\mu_o}{2} H_o^2 \, \ell \, (A_{coil} - A_{cage}) \text{ (Joule)} \tag{3}$$

where the A's are the cross-sectional areas of coil and cage and where $\mu_o = 4\pi \times 10^{-7}$ Henry/m and is the permeability of free space. From (2) the expression becomes

$$E = \frac{\mu_o}{2} \frac{n^2 I^2 (A_{coil} - A_{cage})}{\ell} \tag{4}$$

The energy can also be expressed in terms of the net self-inductance, L, of the assembly by the relation

$$E = \frac{1}{2} L I^2 \tag{5}$$

On equating (4) and (5) we obtain for the inductance

$$L = n^2 \mu_o \frac{(A_{coil} - A_{cage})}{\ell} \text{ (Henry)} \tag{6}$$

The cage, therefore, reduces the inductance of the coil by a factor $(A_{coil} - A_{cage})/A_{coil}$.

The cage also adds some series resistance to the coil. The circumferential current, i, in a tube of the cage is distribution in depth, x, into the copper according to the approximate formula

$$J = \frac{i}{\delta} e^{-x/\delta} \tag{7}$$

where J is the current density (A/m), and δ is the skin depth, given by the relation

$$\delta = \sqrt{\frac{1}{\pi\mu_o f\sigma}} = \sqrt{\frac{2}{\mu_o\omega\sigma}} \tag{8}$$

Here f is the frequency (Hz) and σ is the conductivity of copper (mhos/m).

The power dissipated per unit area of tube surface is then

$$W'' = \int_0^\infty \frac{J^2}{\sigma}\,dx = \frac{i^2}{2\sigma\delta}\ (\mathrm{W/m^2}) \tag{9}$$

The total power for N tubes of height, h, and diameter, D, is

$$W = \frac{N\,\pi D\,h\,i^2}{2\sigma\delta} = \frac{n^2\,N\pi\,Dh\,I^2}{2\sigma\ell^2\delta} \tag{10}$$

and the effective series resistance introduced into the coil is therefore

$$R = \frac{n^2\,N\pi\,Dh}{2\sigma\ell^2\delta} \tag{11}$$

We have assumed that $h < \ell$. If the tubes are longer than the coil, h, in (11), is replaced by ℓ.

A.2 HEAT INPUT TO THE CHARGE

We assume for mathematical convenience that the charge has the shape of an oblate spheroid, which is a good approximation to the actual disc-like shape. The equation of the surface is

$$\frac{r^2}{a^2} + \frac{z^2}{c^2} = 1 \tag{12}$$

where a and c are the semi-axes of the spheroid, and z and r are vertical and horizontal cylindrical coordinates.

The distribution of induced current in the spheroid depends strongly on the skin depth, δ, in the molten material. The two limiting cases, $\delta >> c$ and $\delta << c$, are mathematically tractable, while the intermediate case, $\delta \sim c$, is too difficult for analytical treatment. The limiting cases, however, serve to bracket the intermediate case and give considerable insight into the general problem.

A.2.1 Large Skin Depth

When $\delta >> c$, the uniform magnetic field, H_o, produced by the coil, penetrates the charge with little distortion. Under these conditions the induced circumferential electric field, E_θ, is given by the simple circuital emf equation

$$2\pi r^2 E_\theta = -\frac{\partial}{\partial t}(\pi r^2 B) = -\pi r^2 \mu_o j\omega H_o \tag{13}$$

where $\pi r^2 B$ is the instantaneous magnetic flux through a circle of radius, r, and ω is the angular frequency.

The associated current density is

$$J_\theta = \sigma E_\theta = -\frac{1}{2}\sigma\mu_o \omega r H_o \tag{14}$$

The rate of heat generation per unit volume at the radius, r, is

$$W''' = \frac{1}{\sigma}|J_\theta|^2 = \frac{1}{4}\sigma\mu_o^2 \omega^2 r^2 H_o^2 \tag{15}$$

The power per unit area projected on the (x,y) plane is, from (12),

$$W'' = 2z W''' = \frac{1}{2}\sigma\mu_o^2 \omega^2 H_o^2 c r^2 \sqrt{1 - \frac{r^2}{a^2}} \tag{16}$$

It is to be noted that W" is zero at both r = 0 and r = a and is maximum at $r = a\sqrt{2/3} = 0.816a$.

The total heating rate for the whole ellipsoid is

$$W = \int_0^a W'' \, 2\pi r dr = \frac{2\pi}{15} \sigma \mu_o^{2} \omega^{2} a^4 c H_o^{2} \tag{17}$$

From (8), this can also be written, in terms of instead of a, as

$$W = \frac{4\pi}{15} \frac{\mu_o \omega a^4 c H_o^2}{\delta^2} \tag{18}$$

As a numerical example we take the following values:

$$\begin{aligned} \mu_o &= 4 \times 10^{-7} \text{ H/m} \\ f &= 10 \times 10^{6} \text{ MHz} \\ a &= 0.04\text{m} \\ c &= 0.01\text{m} \\ \delta &= 2c = 0.02\text{m} \\ H_o &= 1000 \text{ A/m} \end{aligned}$$

Then $W = 4000$ watts.

The value chosen for δ corresponds to $\sigma = 63$ mho/m and is probably near the limit of validity of the theory. The value of H_o corresponds to that for a 5-turn coil of length 10cm carrying a current of 20 amperes.

A.2.2 Small Skin Depth

The case, $\delta << c$, may not occur in practice for the range of conductivities likely to be found for molten refractory materials without the use of frequencies well in excess of 10 megahertz. However, it is still of value to determine the power distribution in the charge for this limiting case.

Like the cage tubing, the spheroid acts like a nearly perfect diamagnetic body when $\delta << c$. The current distribution on the surface of the spheroid is such that the external magnetic field is the same as that produced by a uniformly magnetized body of the same shape. The intensity of magnetization, m, (dipole moment per unit volume) is related to the applied field, H_o, of the coil by the formula

$$m = \frac{H_o}{1-N} \tag{19}$$

where N is the demagnetization factor, which depends on the ellipsoid shape. For a sphere $N = 1/3$. For an oblate spheroid with semi-axes, a, a, c, the factor is given by[1]

$$N = \left(\frac{1 + k^2}{k^2}\right)\left(1 - \frac{1}{k}\tan^{-1} k\right) \tag{20}$$

where

$$k = \sqrt{\frac{a^2}{c^2} - 1} \tag{21}$$

Table A.1 shows how N varies with c/a.

TABLE A.1

DEMAGNETIZATION FACTOR N

c/a	N
0.0	1.000
0.2	0.750
0.4	0.588
0.6	0.478
0.8	0.396
1.0	0.333

For the shape of interest here, where $c/a = 1/4$, $N = 0.7037$. For this value the intensity of magnetization is from (19)

$$m = -3.375\ H_o \tag{22}$$

Knowing m, and therefore the effective distribution of magnetic charge density over the surface of the spheroid, one can calculate the magnetic field distribution and from it the equivalent surface current distribution.

In Figure A.2 we consider the ellipsoid as a perfect diamagnetic body with permeability $\mu = 0$. Then the magnetic induction, B_i, within the ellipsoid is given by

$$B_i = \mu H_i = 0 \tag{23}$$

Also,

$$B_i = H_i + m \tag{24}$$

The directions of H_i and m are shown in Figure A.2.

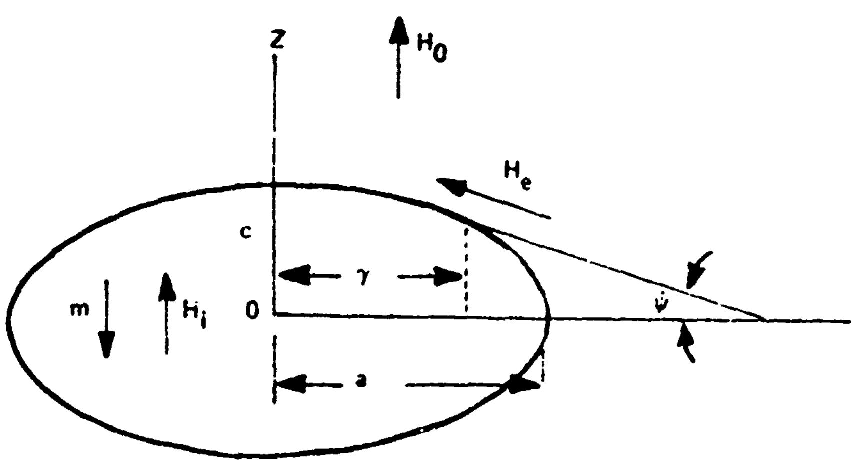

THE ELLIPSOID AS A PERFECT DIAMAGNETIC BODY

FIGURE A.2

We now apply the boundary condition that the tangential component of H is continuous. Now the field, H_e, just outside the ellipsoid is known to be tangential, as indicated in Figure A.2. Therefore, just below the surface, $(H_i)_{tan} = H_e$, as shown in the vector diagram in Figure A.3 where the vector sum of H_e and H_n equals the internal field, H_i.

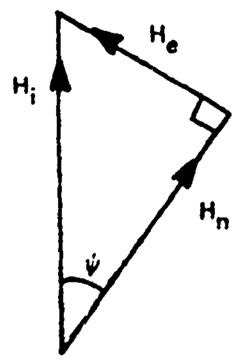

MAGNETIC FIELD VECTORS

FIGURE A.3

From the diagram we obtain the result

$$H_e = H_i \sin \psi = - m \sin \psi \tag{25}$$

where the angle, ψ, is defined in Figure A.2.

On substitution for m from (19) we find that

$$H_e = \frac{H_o \sin \psi}{1-N} \tag{26}$$

The surface current, i, in A/m is equal to the tangential magnetic field. It is therefore given by

$$i = \frac{H_o \sin \psi}{1-N} \tag{27}$$

To evaluate $\sin \psi$, we represent the ellipsoid by the parametric equations

$$r = a \cos \phi \tag{28}$$

$$z = c \sin \phi \tag{29}$$

Then

$$\sin \psi = \frac{dz}{ds} \tag{30}$$

where ds is an element of arc on the allipsoid at the point of tangency in Figure A.2 and is given by

$$ds = \sqrt{dr^2 + dz^2} \tag{31}$$

From (28) and (29),

$$dr = - a \sin \phi \, d\phi \tag{32}$$

$$dz = c \cos \phi \, d\phi \tag{33}$$

Therefore

$$ds = d\phi\sqrt{a^2 \sin^2 \phi + c^2 \cos^2 \phi} \tag{34}$$

On substituting for dz and ds from (33) and (34) into (30), we obtain

$$\sin \psi = \frac{c \cos \phi}{\sqrt{a^2 \sin^2 \phi + c^2 \cos^2 \phi}} \tag{35}$$

Therefore, from (27),

$$i = \frac{H_c}{1-N} \frac{c \cos \phi}{\sqrt{a^2 \sin^2 \phi + c^2 \cos^2 \phi}} \tag{36}$$

The total power is

$$W \;=\; R_s\ i\ \ 2\ \ rds \tag{37}$$

where R_s, the surface resistance in ohm/ , is given by (9) as

$$R_s \;=\; \frac{W''}{i} \;=\; \frac{1}{2} \tag{38}$$

On substituting for i, r, ds, and R_s from (27), (28), (34) and (38) into (37), we find

$$W \;=\; \frac{ac\ \ H_o}{(1-N)} \int_{-\frac{}{2}}^{/2} \frac{\cos\ \ d}{a\ \ \sin\ \ \ + c\ \ \cos} \;=\; \frac{a\ H_o}{} \cdot \frac{c\ F(\frac{a}{c})}{a(1-N)} \tag{39}$$

where

$$F(x) \;=\; \frac{(2x\ -1)}{(x\ -1)^{3/2}} \log_e\ (\ x\ -1 + x) \;-\; \frac{x}{x\ -1} \tag{40}$$

Table A.2 shows how the second factor in (39) depends on a/c. It can be seen that the power is quite constant for c/a between 0.1 and 1.0 (for fixed a). For very flat ellipsoids the power increases slowly.

TABLE A.2

GEOMETRICAL FACTOR IN EQUATION 39

c/a	$\frac{c\ F(\frac{a}{c})}{a(1-N)}$
0.0001	24,020
0.001	18.101
0.01	12.534
0.1	8.190
0.2	7.510
0.25	7.465
0.4	7.564
0.6	8.121
0.8	8.744
1.0	9.425

The radial distribution of the power is also of interest. From (37) we find, on counting the power on both top and bottom of the ellipsoid, that

$$\frac{dW}{dr} = \frac{4\, R_s H_o C}{(1-N)} \cdot G\left(\frac{r}{a}\right) \tag{41}$$

where

$$G\left(\frac{r}{a}\right) = \frac{\left(\frac{r}{a}\right)^3}{\sqrt{\left[1 - \left(1 - \frac{c^2}{a^2}\right)\frac{r^2}{a}\right]\left[1 - \left(\frac{r^2}{a}\right)\right]}} \tag{42}$$

Table A.3 shows how G varies with r/a for the case c/a = 1/4. The last column in the table gives the fraction of the power within a radius r. It is seen that the power is strongly concentrated at the equator of the ellipsoid.

TABLE A.3

RADIAL DISTRIBUTION OF POWER FOR c/a = 1/4

$\frac{r}{a}$	$G(\frac{r}{a})$	$\frac{W(r)}{W(a)}$
0.0	.0000	.0000
0.1	.0010	
0.2	.0083	.0001
0.3	.0296	
0.4	.0757	.0021
0.5	.1650	
0.6	.3317	.0121
0.7	.6532	
0.8	1.3492	.0549
0.9	3.4094	
1.0	∞	1.0000

For c/a = 1/4 the total power, from (39) and Table A.2, is

$$W = 7.47 \frac{H_o^2 a^2}{\sigma \delta} = 7.47\, H_o^2 a^2 \sqrt{\frac{\omega \mu_o}{2\sigma}} \tag{43}$$

We expect that this expression will remain approximately valid for $\delta = c/2 = 0.005$m. At $f = 10$ megahertz, this corresponds to $\sigma = 1000$ mho/m. For $a = 0.04$m and $H_o = 1000$ A/m, as before, we find from (43) that $W = 2400$ watts which is to be compared with the value of 4000 watts calculated on the $\delta >> c$ assumption for $\delta = 0.02$m.

On substituting for σ from (8) we find that (43) takes the form

$$W = 3.73\ \mu_o\ \omega\ a^2\ H_o^{\ 2}\ \delta \tag{44}$$

which shows that W tends to zero for very small δ, for constant ω. The limiting expressions, (44) and (18), therefore show that as δ varies from small to large values, due to variation of the conductivity, W passes through a maximum which, for the numerical values chosen above, probably lies between 2000 and 4000 watts and occurs for $\delta = c = 0.01$m. It is to be noted that for constant σ, W increased with increasing ω, as can be seen from (43).

A.3 COIL RESISTANCE DUE TO LOAD

On substituting for H_o from (2) into (44), we can express W in terms of the current I in the coil by the formula

$$W = \frac{4.78\ \mu_o\ \omega\ a^2\ \delta\ n^2\ I^2}{\ell^2} \tag{45}$$

The load therefore acts like a resistance

$$R_L = \frac{4.78\ \mu_o\ \omega\ a^2\ \delta\ n^2}{\ell^2}\ (\delta << c) \tag{46}$$

Likewise, from (18) we obtain

$$R_L = \frac{4\pi}{15}\frac{\mu_o\ \omega\ a^4\ c\ n^2}{\ell^2\delta^2}\ (\delta >> c) \tag{47}$$

A.4 STARTUP

In order to start the inductive heating one must usually add some high conductivity material such as particles of the same metal as is present in the composition of the charge itself. Typically, the metals used are available in the form of random-sized small chunks, flakes or chips and for purposes of our calculations we have assumed the particles to be spherical with radius a and conductivity σ. In the high frequency field, H_o, the sphere acts as a diamagnetic body with a demagnetization factor $N = 1/3$ (see Table A.1). From (19) the effective intensity of the magnetization of the sphere is

$$m = -\frac{3}{2} H_o \tag{48}$$

The total magnetic moment of the sphere is

$$M = \frac{4}{3} \pi a^3 m = -2\pi a^3 H_o \tag{49}$$

For the special case of the sphere, unlike that of a spheroid, the moment, M, acts as though it were located at the center of the sphere. The tangential magnetic field at the surface of the sphere, due to M, is

$$(H_o)_{dipole} = \frac{M \sin \theta}{4\pi a^3} = -\frac{1}{2} H_o \sin \theta \tag{50}$$

where θ is the angle between the radius vector and the z-axis.

Since the applied field, H_o, gives a tangential component, $-H_o \sin \theta$, at the surface of the sphere, the total tangential field is

$$H_t = -\frac{3}{2} H_o \sin \theta \tag{51}$$

The circumferential current per unit length on the sphere is therefore

$$i_\phi = -\frac{3}{2} H_o \sin\theta \qquad (52)$$

since it equals the discontinuity in H_o at the surface of the sphere.

The surface resistance R_s is given by (38). On multiplying this by i_ϕ^2 and integrating over the area of the sphere, we obtain for the power input to the sphere

$$W = \int_0^\pi \left(\frac{1}{2\sigma\delta}\right)\left(\frac{9}{4} H_o^2 \sin^2\theta\right) 2\pi a^2 \sin\theta d\theta = \frac{3 H_o^2 a^2}{\sigma\delta} \qquad (53)$$

It is of interest to consider that this power is balanced by blackbody radiation from the surface of the sphere at absolute temperature, T_o, with the surroundings at temperature, T. Then

$$4\pi a^2 \sigma_o(T^4 - T_o^4) = \frac{3\pi H_o^2}{\sigma\delta} \qquad (54)$$

or

$$\sigma_o(T^4 - T_o^4) = \frac{3 H_o^2}{4\sigma\delta} \qquad (55)$$

where $\sigma_o = 5.672 \times 10^{-8}$ W m^{-2} deg^{-4} is the Stefan-Boltzmann constant. (55) shows that the equilibrium temperature is independent of the radius of the sphere. For the case of a field, H_o = 1000 A/m, as before, and with $\sigma = 5.0 \times 10^{-5}$ mho/m, $\sigma_o(T^4 - T_o^4) = 1500$ W/m^2, and T = 431 K. The metal sphere would therefore not melt for the field assumed. However, for a ten times greater field of 10,000 A/m, which is not unreasonable, we get

$$\sigma_o(T^4 - T_o^4) = 150{,}000 \text{ W/m}^2$$

and

$$T = 1276 \text{ K}$$

which will melt certain metals.

A more appropriate assumption for skull melting is that the metal sphere is embedded in a powder of thermal conductivity K. Then the equilibrium temperature is given by

$$T - T_o = \frac{W}{4\pi Ka} \tag{56}$$

For $K - 0.1$ watt/(m deg K), $a - 1 \times 10^{-3}$m, $H_o = 10{,}000$ A/m, and the other constants the same as before, we find that $W = 1.88$ watts and $T = 1600°K$. The particle would therefore raise the temperature of the surrounding powder to a value where inductive heating of the powder would occur.

A.5 SCALING LAWS

It is on considerable interest to determine the scaling laws for magnetic field H_o and the power input W when the geometry of the skull and the charge are changed by some linear factor. To find the scaling laws we assume that the rate of heat loss from the molten charge to the surroundings is given approximately by the usual formula

$$W_{Loss} = h\, A_m\, (T_m - T_o) \tag{57}$$

where h is the heat transfer coefficient, A_m is the surface area of the melt, T_m is the temperature of the melt, and T_o is the temperature of the surroundings. Since h, T_m and T_o are constant for a given material, (49) can be written as

$$W_{Loss} \propto a^2 \tag{58}$$

where a, as above, is the major semi-axis of the spheroidal melt. It is assumed that the shape of the melt remains fixed, so that c/a is constant.

Under equilibrium conditions the total power W supplied to the molten charge equals the rate of heat loss.

Therefore

$$W = W_{Loss} \tag{59}$$

In the case where the skin depth δ is large compared with a, we find from (18), (50) and (51) for constant ω and σ,

$$H_o \propto \frac{1}{a^{3/2}} \tag{60}$$

This means, for example, that if the geometry is scaled down by a linear factor of 2, H_o (the high frequency field) has to be increased by a factor of $2\sqrt{2} = 3.83$. A linear factor of 4 requires an eightfold increase in H_o.

On the other hand, in the case of a highly conductive melt, (31) along with (50) and (51), shows that

$$H_o = \text{constant} \tag{61}$$

From (50) and (51) the scaling law for power input is simple

$$W \propto a^2 \tag{62}$$

whatever the skin depth may be. However, in the case of large δ, since the power must be transferred at a higher value of H_o, and therefore higher coil current, the coil losses are larger in this case and the efficiency is therefore lower.

A.6 RELATION TO PREVIOUS WORK

The foregoing theoretical analysis and the following thermal analysis and power control analysis, together constitute a more detailed study of the process outlined in a recent paper by Aleksandrov et al.[3] The results of the study generally support the conclusions of the Russian authors and serve to sharpen their criteria for stable operation of the skull melting technique.

APPENDIX B

THEORY OF THE THERMAL CHARACTERISTICS OF SKULL MELTING

It has been established already that the currents produced in an oblate spheroid by an induction heater are largely concentrated around an equatorial ring which is located near the surface. While the current density as a function of position has been derived rigorously only for the oblate spheroid, the results for this case give us much insight and enable us to anticipate what will probably happen in the case of a more complicated body of revolution whose radius is large compared with its thickness in the axial direction and which is an electrical conductor.

Qualitatively speaking, we may say that the currents in the body will establish themselves in such a way as to exclude most of the field impressed by the induction heater coil. The value of B produced by a ring of current depends mainly on the current, and not so much on the radius of the ring (in a solenoid, the value of H is independent of the radius of the coil), whereas the total flux produced is the product of the area of the ring and the average value of B within the ring. Therefore, in the case of a conductor which is a flattened convex body of revolution, one may expect that the induced current will be largely concentrated in a ring of the largest possible radius which is contained in the body. It is probably best to leave this kind of qualitative argument in its present rather vague state, and simple to conclude that it is of interest to study the shape of the isotherm at the melting temperature in a region filled with a powder of low thermal conductivity, which contains a ring source and which is fairly closely contained by a vessel (represented by an isotherm at 300°K) maintained at room temperature. We will also suppose that near the top of the vessel a rather large amount of heat is lost in order to simulate the conditions that must obtain when the crystal is being pulled slowly from the melt through an aperture above.

One way to approach the problem is to take the shape of the 300K isotherm from the drawing of the tubes containing the coolant and to solve rigorously the boundary value problem thus defined. However, the physical parameters involved (for example the thermal conductivity of the powder, which will depend upon its packing and any sintering that may take place) are very poorly known, so it is not justified to use such rigorous procedure. Instead we may employ a simpler technique and obtain at least a preliminary understanding of the effects on the molten zone that will be produced by variations in the main features of the system. Without great difficulty some important results can thus be obtained which will serve as guide posts in the experimental program.

In doing the simplified problem we are at liberty to place sources and sinks of various strengths at such locations as we choose, provided that these locations are outside the region of interest, which we will take to be bounded by the 300K isotherm. Of course the ring source, which is used to model the induction heating, must be within the melt. We make use of external sources and sinks to model the loss of heat from the top and to control the shape of the 300K isotherm.

It appears that the 300K isotherm must pass close to the ring source in that melt in order to give the isotherm at the melting point its expected flat shape. Also, we want the 300K isotherm to be close to the melt at the top (to model the loss of heat through the aperture used to extract the crystal) and otherwise to resemble, at least roughly, the shape of the cup formed by the tubes containing the coolant.

In Figure B.1 we show what we have taken to be the "standard" arrangement for the 300K and 2318K isotherms (the melting point of alumina is 2318K). The positions of the sources and 3 sinks are shown and the drawing is to scale, as indicated. The arrangement pictured in Figure B.1 was obtained after a number of mathematical experiments; one lesson that was learned very early is that the 300K sink on the axis has a drastic effect on the shape of the melt, and that the lower surface of the melt needs to be well insulated. The melt is, in effect, acting as a fin, with the heat traveling towards the center and being lost along the way. The insulation along the under side, which serves to keep the heat loss to a minimum, can be obtained by making sure that the molten zone is in the top part of the cooled container, so that a thick blanket of powder is left unmelted beneath the 2318K isotherm.

We will now illustrate the sensitivity of the shape of the molten region to changes in some of the system parameters by means of figures which show the two standard isotherms and two slightly distorted isotherms. The distorted isotherms are obtained by solving the problem with some changes in the boundary conditions.

In Figure B.2 we show two pairs of isotherms to demonstrate the sensitivity of the shape of the melt to a variation in the position of the upper part of the 300K isotherm from the standard position. The lower part of the 300K isotherm has been held nearly in place. It is clearly seen that the top surface of the melt moves further than the 300K isotherm, while even the bottom part suffers a significant displacement. It is of interest to note that the changes seen are due mainly to a change of 50 watts in the strength of the sink on the axis (from 300W to 250W).

In Figure B.3 we show two pairs of closely spaced isotherms. The lower part of the 300K isotherm has been caused to move about 3mm below its standard position (on the axis), but the corresponding variation in the position of the 2318K isotherm is only about 1mm at the bottom and nearly nothing at the top of the melt. Thus it is seen that the shape of the molten zone is not very sensitive to variations in the geometry of the bottom of the cup, provided that the blanket of insulation is present.

We also determined the sensitivity of the shape of the molten zone to a change in the input power (supplied by the induction heater) by raising the strength of the ring source from 3150W to 3300W, while the shape of the 300K isotherm was kept essentially the same as the standard. The result is shown in Figure B.4, which indicates that the shape of the melt is only slightly affected by the change in power input. This is probably due to the fact that the distance between the side of the molten zone and the cold container is very small, so a minute change in this dimension is all that is needed to cause most of the added power to flow directly into the container walls near the plane $z = 0$.

Under certain circumstances it might be desirable to let the molten mass cool slowly, of its own accord, without penetrating the layer of powder that lies over the melt. In such a case one might obtain a symmetrical melt, as shown in Figure B.5.

So far, we have discussed only the case of molten alumina. Another material of interest is zirconia, whose melting point is 2988K. In Figure B.6 we show a set of sources and sinks and the corresponding isotherms at 2988K and 300K. Because of its higher temperature the upper surface of the pool of molten zirconia may be expected to lose much more heat by radiation than is the case with alumina. To allow for this, the strength of the point sink has been set at 800W, and the strengths of the other sources and sinks adjusted in an attempt to produce a suitable configuration of the 2988K and 300K isotherms. While the amount of mathematical experimentation with the model of the higher melting point material has been very limited, we expect that it would be necessary to separate the ring source slightly further from the main ring sink in order to produce a 2988K isotherm that is similar in appearance to the 2318K isotherm of Figure B.1. From an operational point of view, this means that the frequency of the induction locater must be set so as to obtain a large skin depth in the melt.

We expect that the sensitivity of the shape of the zirconia melt to changes in the external configuration will be qualitatively the same as in the case of the alumina melt already discussed.

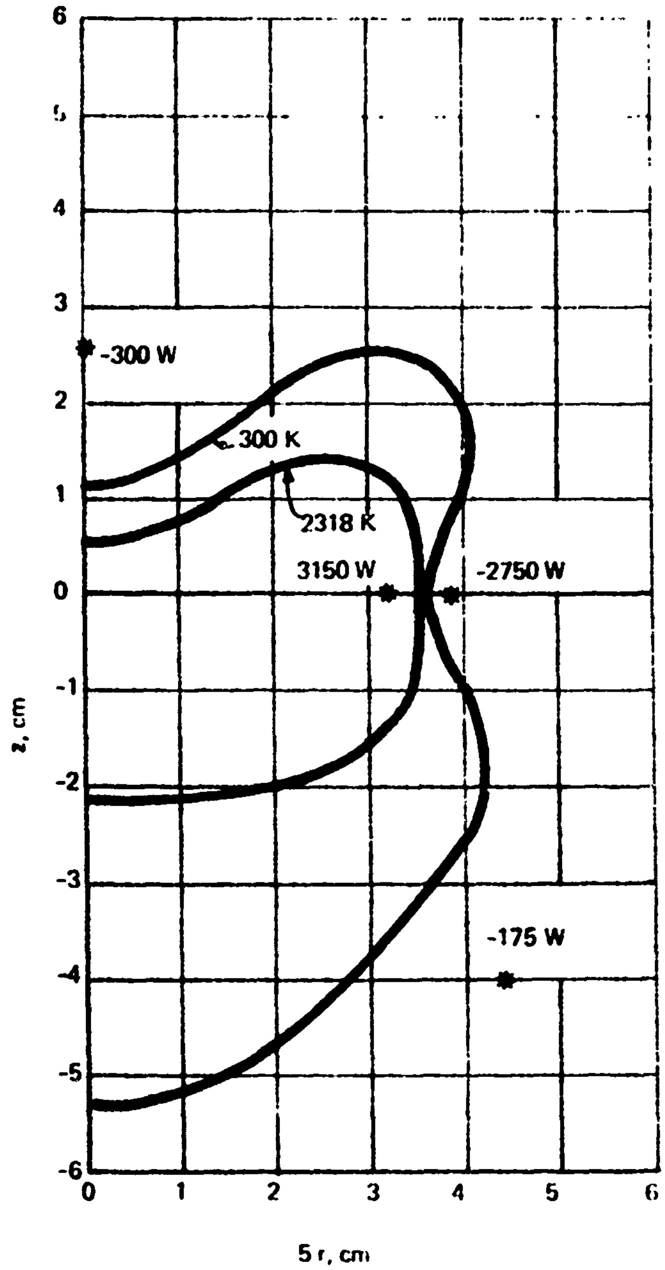

FIGURE B.1 ISOTHERMAL PROJECTION

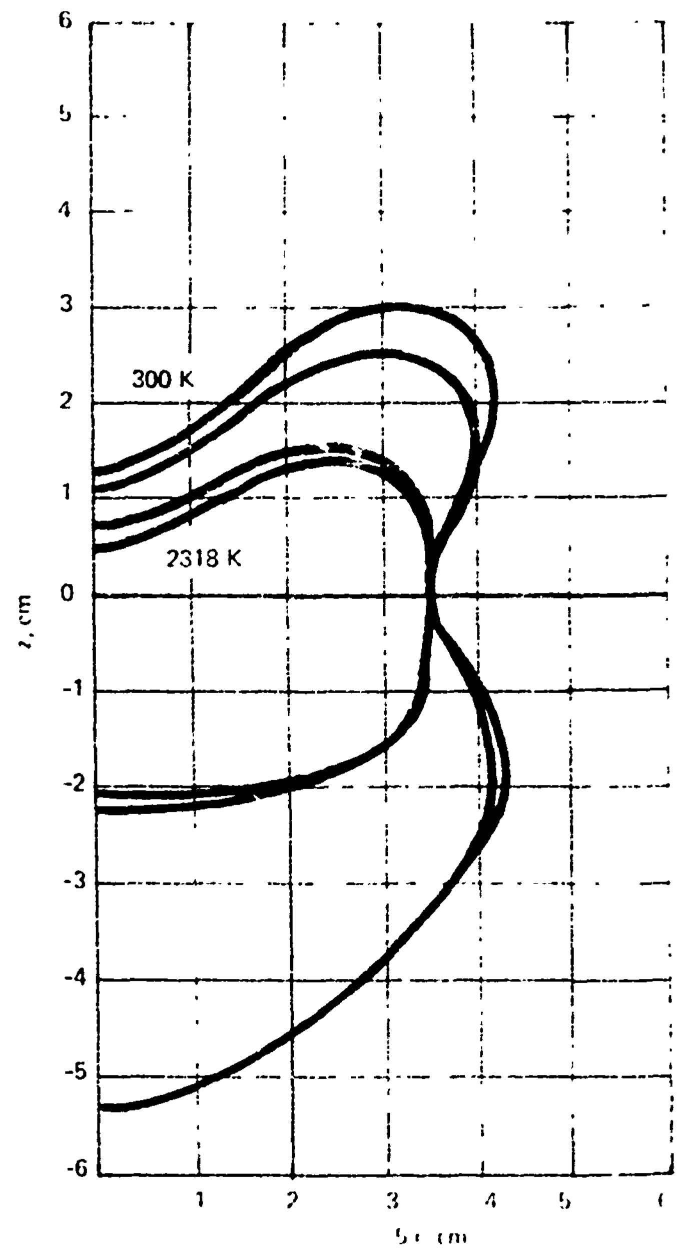

FIGURE B.2 ISOTHERMAL PROJECTION

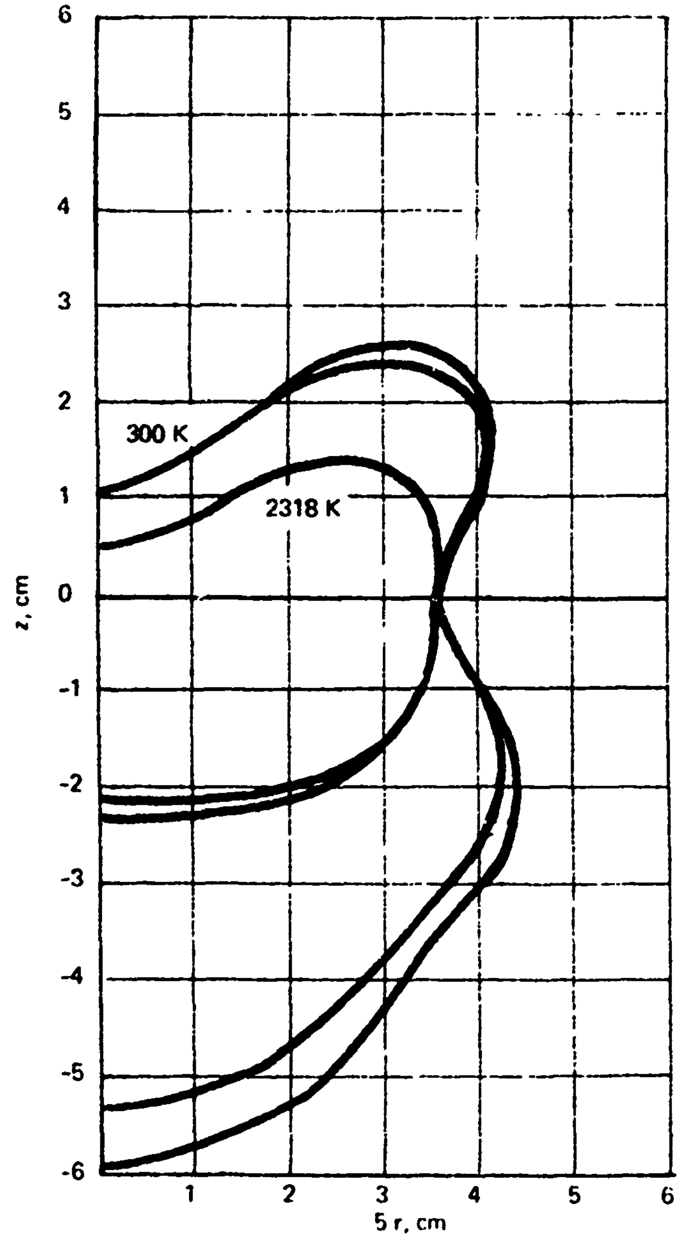

FIGURE B.3 ISOTHERMAL PROJECTION

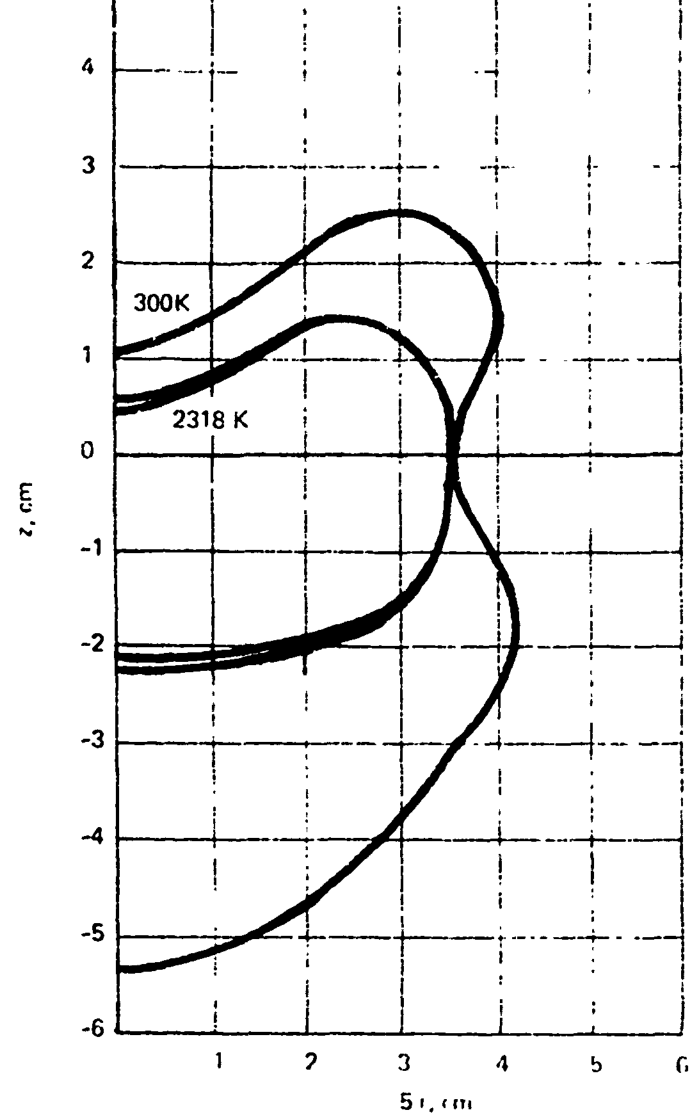

FIGURE B.4 ISOTHERMAL PROJECTION

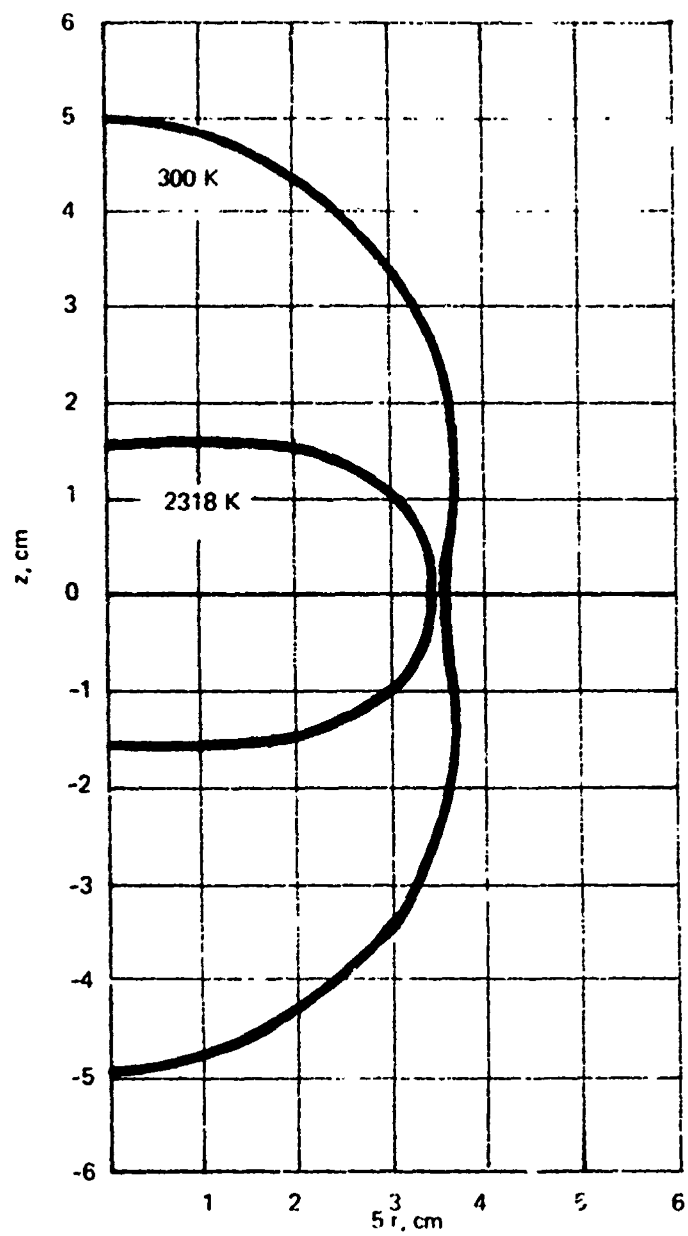

FIGURE B.5 ISOTHERMAL PROJECTION

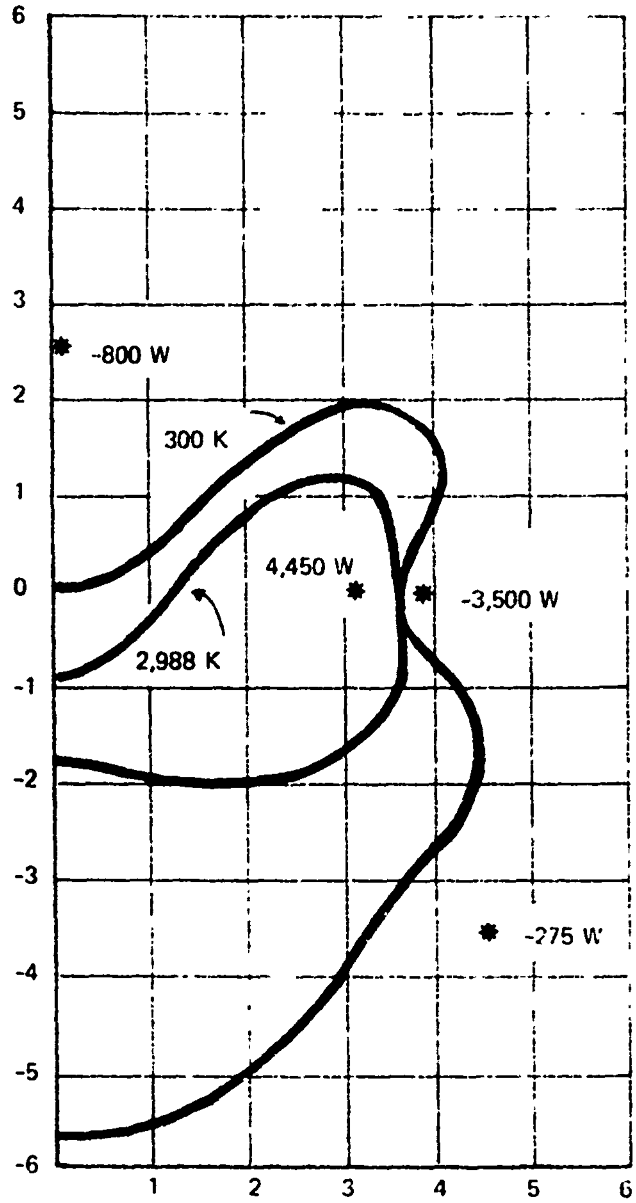

FIGURE B.6 ISOTHERMAL PROJECTION

APPENDIX C

TEMPERATURE DISTRIBUTION DUE TO A RING SOURCE

In this section we derive the formula for the temperature (in steady state) at a point in an infinite medium which contains a source of heat in the form of a ring. We assume the thermal conductivity of the medium to have the fixed value K (watts cm^{-1} deg C^{-1}), so the temperature must satisfy Laplace's equation

$$\nabla^2 T = 0$$

and furthermore we require that the temperature be zero at infinity.

In accordance with these assumptions we find the temperature, dT, at a field point, P, whose coordinates are (x,y,z) produced by a point source of strength dQ watts located at P' with coordinates (x',y',z') to be

$$dT = \frac{dQ}{4\pi Ks} \tag{1}$$

where

$$s = \sqrt{(x-x')^2 + (y-y')^2 + (z-z')^2} \tag{2}$$

By adding up the contributions due to many such sources we can, at least in principle, find the temperature due to any distribution of heat sources.

In Figure C.1 we show a ring source of radius, a, located in the z-plane and a field point at an arbitrary point. It is evident from the diagram that

$$\begin{aligned} x' &= a \cos \theta \\ y' &= a \sin \theta \\ z' &= 0 \end{aligned} \tag{3}$$

Now suppose the source to dissipate Q' watts cm^{-1} uniformly along its circumference. Then

$$dQ = Q' \, a d\theta \tag{4}$$

since ad is the element of arc. Therefore we find from the above equati equation

$$dT = \frac{Q' \, a \, d\theta}{4\pi K \sqrt{(x - a \cos \theta)^2 + (y - a \sin \theta)^2 + z^2}} \tag{5}$$

or, by integration of (5) around the loop,

$$T = \frac{Q'a}{4\pi K} \int_0^{2\pi} \frac{d\theta}{\sqrt{(x - a \cos \theta)^2 + (y - a \sin \theta)^2 + z^2}} \tag{6}$$

On account of the symmetry of the problem we can replace x in (6) by r and replace y by 0. Thus

$$T = \frac{Q'a}{4\pi K} \int_0^{2\pi} \frac{d\theta}{\sqrt{r^2 + a^2 + z^2 - 2ar \cos \theta}} \tag{7}$$

The integral in the right-hand side of (7) is not "elementary", but can be evaluated simply in terms of the well known complete elliptic integral, $\overline{K}(m)$, which is defined by the formula

$$\overline{K}(m) = \int_0^{\pi/2} \frac{d\phi}{\sqrt{1 - m \sin^2 \phi}} \tag{8}$$

First make the substitution

$$\theta = 2\phi + \pi$$

in (7) to obtain

$$T = \frac{Q'a}{2\pi K} \int_{-\pi/2}^{\pi/2} \frac{d\phi}{\sqrt{(a + r)^2 + z^2 - 4ar \sin^2 \phi}} \tag{9}$$

Next remove the factor $(a + r)^2 + z^2$ from the expression whose square root is indicated and note, since $\sin^2 \phi$ is even, that the range of integration can be reduced by setting the lower limit to zero if a factor of two is placed in front of the integral. Thus we find

$$T = \frac{Q'a}{\pi K\sqrt{(a + r)^2 + z^2}} \int_0^{\pi/2} \frac{d\phi}{\sqrt{1 - \frac{4ar}{(a + r)^2 + z^2} \sin^2 \phi}} \tag{10}$$

Whence, by the definition of (8), it is clear that

$$T = \frac{Q'a}{\pi K\sqrt{(a + r)^2 + z^2}} \overline{\underline{K}} \left[\frac{4ar}{(a + r)^2 + z^2}\right] \tag{11}$$

The function $\overline{\underline{K}}(m)$ is easily computed by means of the approximations given by Hastings.[5] Finally we let Q be the total heat dissipated by the ring so

$$Q' = Q/2\pi a$$

and

$$T = \frac{Q}{2\pi^2 K\sqrt{(a + r)^2 + z^2}} \overline{\underline{K}} \left[\frac{4ar}{(a + r)^2 + z^2}\right] \tag{12}$$

If the ring is located at a height, h, instead of at the plane, z = 0, the quantity, z, in (12) must be replaced by the quantity, z = h. Note that $\overline{\underline{K}}(0)$ = /2, so a ring source of radius, a = 0, produces a temperature field

$$T = \frac{Q}{4\pi K\sqrt{r^2 + z^2}} \tag{13}$$

This is obviously the field produced by a point source, as it jolly well ought to be.

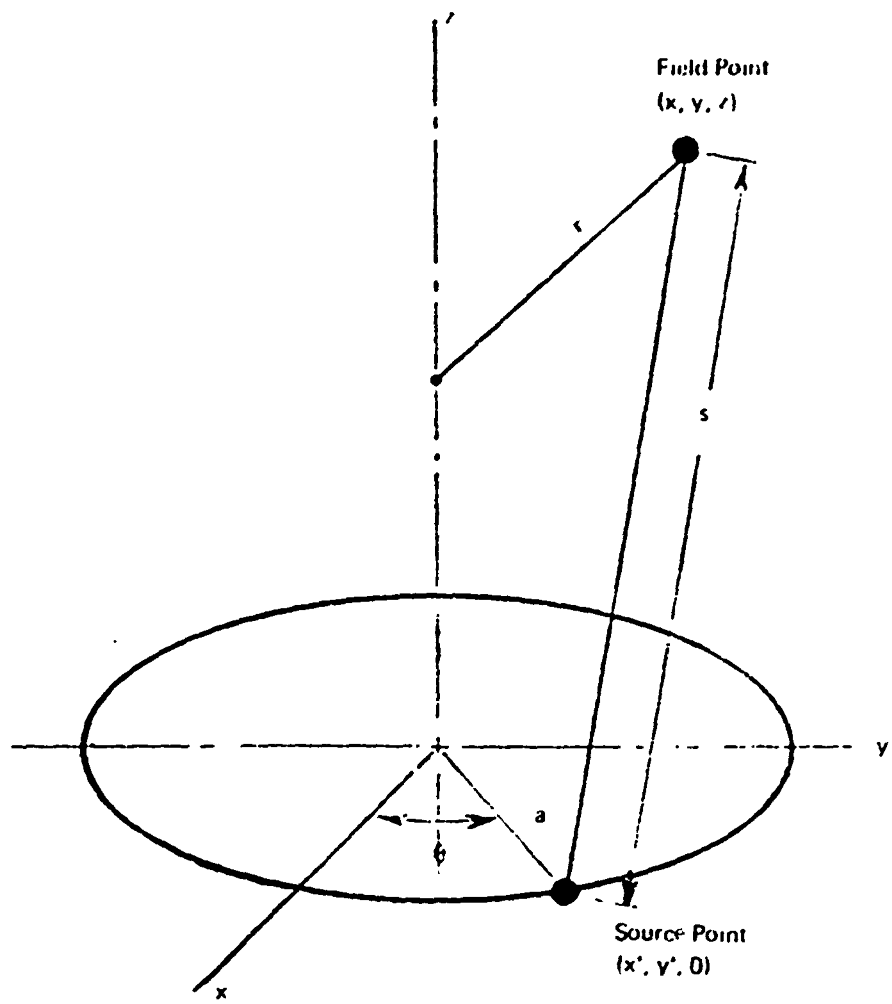

FIGURE C.1 GEOMETRICAL ARRANGEMENT OF THE RING SOURCE & FIELD POINT

APPENDIX D

CONTROL OF RADIO FREQUENCY POWER

The typical current feedback control system, shown in Figure D.1, was used to control the output of the radio frequency generator. The Leeds & Northrup H-AZAR Recorder was used as a preamplifier, the input summing point, and also to record the error signal. The characteristics time constant (τ_1) of the H-AZAR is 0.5 second. The time constants of the RF generator and the associated saturable reactor are approximately this same value or a little longer.

To adjust the controller to the process the integral (reset) action (k_c) of the Leeds & Northrup Series 80 CAT Controller was made as large as possible in order to obtain accurate steady state control, while the gain (k_b) and the derivative (rate) action (k_a) of the controller were adjusted to obtain stable control with minimum response time. The resultant settings were: Reset - 50 repeats/minute, Proportional band = 35%, and Rate = .02 minute. The frequency response of the system is shown in Figure D.2. The open loop response was computed from the measured closed loop response values. The 1/f slope in the low frequency end of the open loop response curve is due to the integral action of the controller. The 65° phase margin, close to the minimum value considered acceptable in good control practice, shows that the adjustment is close to optimum. The closed loop response is good to about 0.3 to 0.7 Hertz. The response does not begin to fall off rapidly until about 1.0 Hertz.

The measurements and adjustment of the control system were difficult because of RF noise pickup. At the operating frequency of about 4 megahertz the inductance of most conductors is not negligible, proper grounding is often impractical and the resultant ground loops lead to excessive pickup. Some effects of RF noise were still noticeable even after our best efforts to improve the system grounding.

Another factor which interfered with closed loop control of the RF power during startup was the dramatic change in conductivity of zirconia upon heating. The conductivity rises rapidly with temperature and there is a correspondingly rapid increase in power absorbed by the load. At the same time there is little change in the RF current because the melt occupies only a small portion of the volume inside the heating coil and also because the penetration depth is still large compared to the dimensions of the melt. The result is a tendency toward thermal runaway.

To solve this problem the Huettinger RF generator was modified to allow the oscillator plate current to be used as the feedback signal. The plate current increased almost in direct proportion to the real power load on the RF generator and is a much better measure of the power into the melt than RF current. Also, this method of control was not sensitive to RF noise pickup. When the control system was adjusted for plate current feedback, the controller settings were: Reset = 100 repeats/ minute, Proportional band = 100%, and Rate = .02 minute. The overall response was not measured but seemed to be about the same as with the RF current feedback.

The last factor in the system dynamics is the thermal transfer function of the charge. This function is difficult to measure but we can estimate the thermal time constant (τ_3) by assuming that the heat loss is entirely due to conduction and using the relationship

$$\tau_3 = C_h \frac{dT}{dW} \qquad (1)$$

The heat capacity, C_h = 4.18 Ms (Joules/degree) in which M and s are the mass and specific heat of the charge, respectively. Typical values are

$$M = 700 \text{ gm}$$
$$s = 0.1 \text{ cal/gm°K}$$

which result in C_h = 293 Joule/°K.

The thermal resistance, dT/dW, is approximately

$$dT/dW \approx \frac{\Delta T}{W} \text{ (degrees/watt)}$$

in which ΔT is the temperature rise of the melt and W is the total input power.

Evaluating this derivative for ΔT = 2600°C and W = 13,000 watts, we obtain dT/dW = .2 degrees per watt per degree and τ_3 = 60 seconds. Since this is much longer than the response time of the closed loop, temperature fluctuations will be considerably smaller than the power fluctuations of the system.

One final consideration is the maximum available power. Power is determined by the magnetic field and therefore by the RF current. The current is determined by the inductive reactance of the coil and the output voltage of the RF generator. Since

$$H = \frac{nI}{\ell}, \quad I = \frac{E}{\omega L} \quad \text{and} \quad L \propto n^2 \tag{2}$$

decreasing the number of turns in the coil, n, increases the current, I, as n^2 and increases the magnetic field, H, and consequently the output power.

Our final coil design is for a 4-turn coil, 2" long and 2.15" mean radius. The coil inductance is given by

$$L = \frac{n^2 r^2}{10 + 9r} = \frac{4^2 \times 2.15^2}{10 \times 2 + 9 \times 2.15} = 1.9 \text{ microhenries} \tag{3}$$

The factor for loss of inductance due to the cross-sectional area of the cage, $(\text{Area}_{\text{coil}} - \text{Area}_{\text{cage}})/\text{Area coil}$, is estimated to be about .8, so that the net inductance is about 1.5 microhenries. Assuming that the maximum voltage is 5,000 volts and at a frequency os 3.6 megahertz, we have

$$I = \frac{5000}{2\pi \times 3.6 \times 10^{6} \times 1.5 \times 10^{-6}} = 150 \text{ amperes}$$

and

$$H = \frac{4 \times 180}{2'' \times 2.54 \times 10^{-2}} = 11{,}600 \text{ amperes/meter.}$$

Substituting this value into (17) from Appendix A,

$$W = \frac{2\pi}{15} \alpha \mu_o^{2} \omega^{2} a^{4} c H_o^{2}$$

with the other parameters

$$\alpha = 50 \text{ mho/meter}$$
$$\mu_o = 4 \times 10^{-7} \text{ henry/meter}$$
$$\omega = 19 \times 10^{6} \text{ radians/second}$$
$$a = .032 \text{ meter}$$
$$c = .01 \text{ meter}$$

we obtain

$$W = 24 \text{ kilowatts}$$

which is half the rated capacity of the RF generator.

In practice we measured 20 kilowatts plate power at approximately these conditions. The power into the cooling water was about 13 kilowatts. This was close to the maximum power obtainable in a practical sense since at higher voltages there was a tendency toward arcing across the work coil.

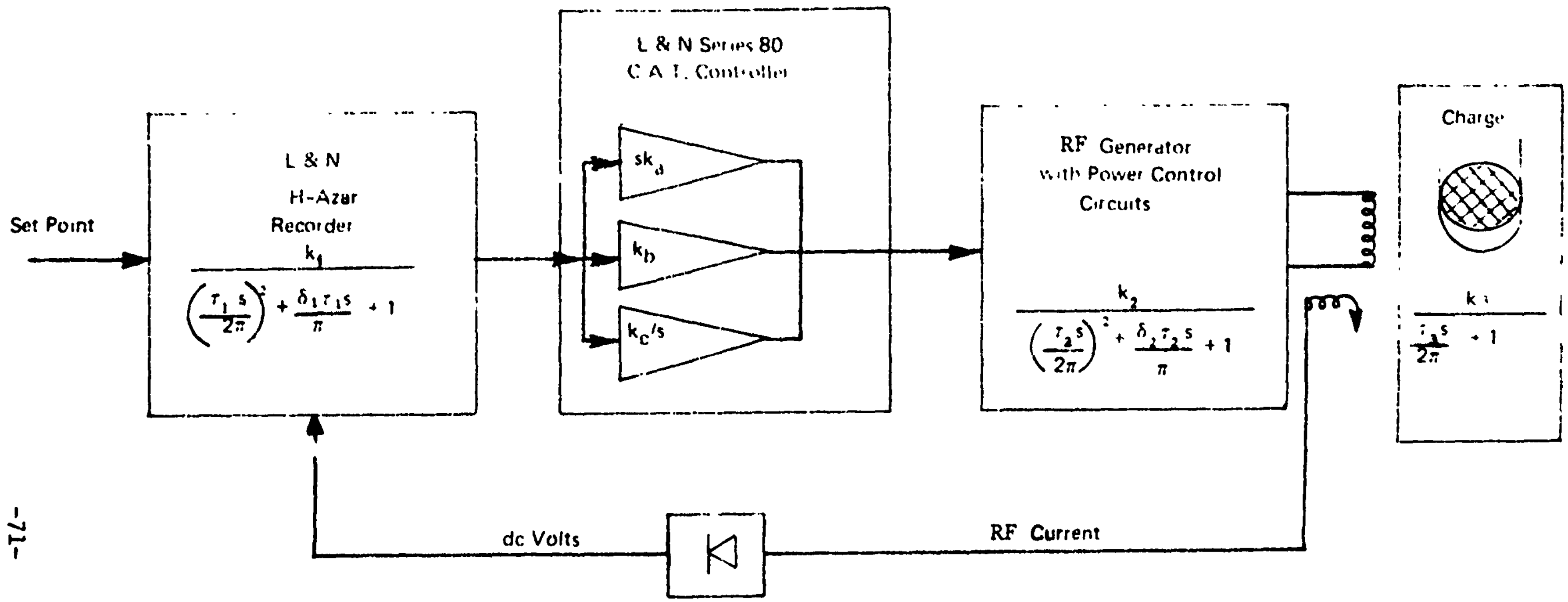

FIGURE D.1 CURRENT FEEDBACK CONTROL SYSTEM

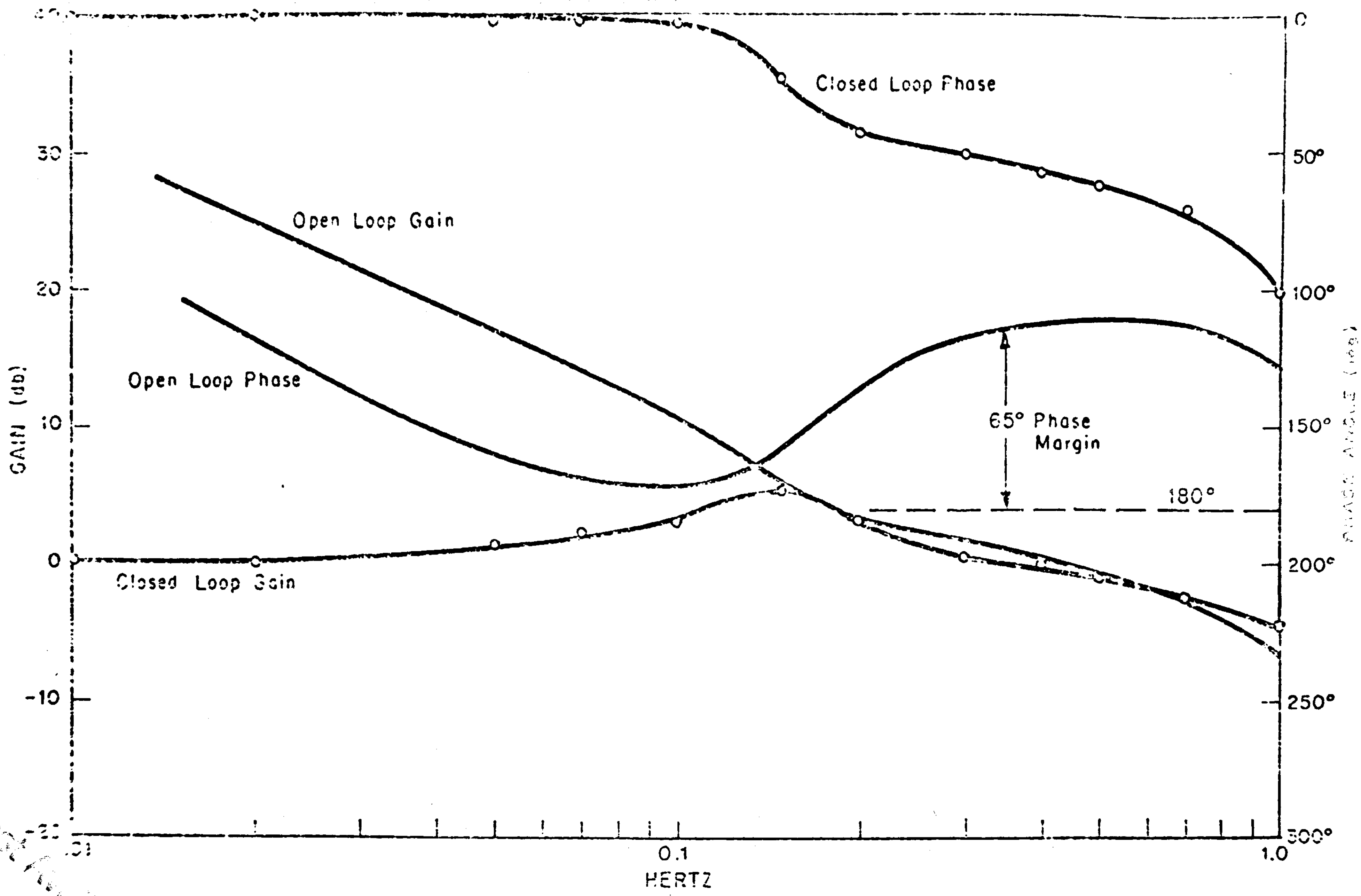

FIGURE D.2 FREQUENCY RESPONSE OF R.F. CURRENT CONTROL SYSTEM

REFERENCES

(1) R.E.W. Casselton, J.S. Thorp and D.A. Wright: Electrical Conduction and Blackening in Yttria-stabilized Zirconia, Proc. British Ceramic Society, No. 19, 1971, pp. 265-77.

(2) L. Heyne and N.M. Beekmans: Electronic Transport in Calcia-stabilized Zirconia, Proc. British Ceramic Society, No. 19, 1971, pp. 229-63.

(3) V.I. Aleksandrov, V.V. Osiko, A.M. Prokhorov and V.M. Tatarintsev: A New Method for Obtaining Refractory Single Crystals and Fused Ceramic Materials, Vestnik Akad. Nauk SSSR, No. 12, 1973, pp. 29-39.

(4) J.C. Maxwell: A Treatise on Electricity and Magnetism, Dover Publications, Inc., 1954, Vol. 1.

(5) C. Hastings, Jr.: Approximations for Digital Computers, Princeton University Press, Princeton, NJ.

(6) J. Reboux (Toco-Stel, Massy, France), private communication.